Bull Volcanol (2016) 78: 38
DOI 10.1007/s00445-016-1030-7

RESEARCH ARTICLE

New insights into the evolution of the magmatic system of a composite andesite volcano revealed by clasts from distal mass-flow deposits: Ruapehu volcano, New Zealand

M. Tost [1,2] · R. C. Price [3] · S. J. Cronin [1,2] · I. E. M. Smith [2]

Received: 23 October 2015 / Accepted: 16 April 2016 / Published online: 21 April 2016

Abstract Stratovolcanoes characteristically build large composite edifices over long periods with stacked lavas intercalated with pyroclastic deposits. In most cases, only the most recent volcanic products are exposed on the flanks of the volcano, and consequently the search for deposits recording an older eruptive and magmatic history is typically focussed far from the cone, within distal tephra deposits. Clasts within lahar and debris avalanche deposits may also provide unique insights into the earliest eruptive and magmatic history of long-lived volcanoes, especially when widespread fallout is absent. Careful sampling and subsequent petrological and geochemical analyses of lava and pumice clasts from six distal mass-flow deposit sequences (hyperconcentrated flow, debris flows and debris avalanche deposits) from Mt. Ruapehu (New Zealand), combined with detailed stratigraphic studies and radiometric age dating, give new perspectives on the pre-50 ka magmatic system of this complex volcano. A conglomerate emplaced between 340 and 310 ka contains evidence for the oldest episode of Mt. Ruapehu volcanism, and unusually for the composite cone, pumice clasts from this unit contain amphibole-bearing xenoliths. Chemical and petrological data for these oldest Ruapehu clasts indicate that a deep (~40 km) crustal storage system had already developed under Mt. Ruapehu before ~340 ka. From the very earliest stages, evolution was largely controlled by magma mixing, along with decoupled assimilation and fractional crystallization within numerous isolated small-scale magma batches stored throughout the crust. From around 340 to 160 ka, there was a progressive shift towards more primitive compositions, suggesting that during this period large-scale replenishment events involving mantle-derived basaltic magmas occurred within the mid- to upper crustal storage system. Subsequent magmas became progressively more evolved due to decoupled fractional crystallization and assimilation processes accompanied by magma recharge events, which triggered major phases of eruptive activity.

Keywords Eruptive activity · Basaltic magmas · Mt. Ruapehu · Mass-flow deposits

Editorial responsibility: V.S. Kamenetsky

Electronic supplementary material The online version of this article (doi:10.1007/s00445-016-1030-7) contains supplementary material, which is available to authorized users.

✉ M. Tost
mtos734@aucklanduni.ac.nz

[1] Volcanic Risk Solutions, Massey University, Palmerston North 4442, New Zealand

[2] School of Environment, University of Auckland, Auckland 1142, New Zealand

[3] Faculty of Science and Engineering, University of Waikato, 3105 Hamilton, New Zealand

Introduction

Stratovolcanoes are large, complex, composite mountains made up of lava and pyroclastic deposits, with associated reworked volcaniclastic deposits that accumulate over hundreds of thousands to millions of years from episodic eruptions (e.g. Coats 1950; Gamble et al. 1999). Published petrological studies of specific volcanoes have often focused on lava samples from young central edifices or cones, but these usually represent only a fraction of the complete eruptive history of the volcano. Volcaniclastic and pyroclastic deposits that form ring plains and fans around the younger edifice generally contain the bulk of erupted material (e.g. Mt. Ruapehu, Mt. Tongariro and Mt. Taranaki, New Zealand, Donoghue et al. 1995, Cronin and Neall 1997, Zernack et al.

2011; Mayon, Philippines, Arguden and Rodolfo 1990; Mt. St Helens, USA, Janda et al. 1981), but the petrology of these deposits has not received the same attention as the lavas of the cones. Consequently, models for the evolution of the magmatic systems feeding long-lived stratovolcanoes based only on cone-sequences are in many cases incomplete.

Lahars and volcanic debris avalanches from stratovolcanoes can transport eruptive products hundreds of kilometres from their volcanic source (e.g. Francis et al. 1985; Stoopes and Sheridan 1992; Vallance and Scott 1997; Mothes et al. 1998; Lecointre et al. 2004). Such mass flows carry with them samples of extensive volcanic sequences that are no longer exposed on the cone. It is only by mapping, studying, dating and sampling this material that the complete eruptive history can be fully documented. Over long periods of geological time, such distal deposits may become the only record of the early geological history of stratovolcanoes, because on the edifices older deposits become buried, eroded or hydrothermally altered (Zernack et al. 2011).

Mt. Ruapehu is one of the most active composite volcanoes in New Zealand, and its eruptives have petrological characteristics similar to those of continental arc lavas worldwide (e.g. Graham and Hackett 1987; Gamble et al. 1999, 2003; Price et al. 2005, 2007, 2012). Petrological and geochemical studies on Mt. Ruapehu have focused on the lava flow sequences exposed on the cone, and these define an eruptive history extending back to ~250 ka (e.g. Cole et al. 1983; Graham and Hackett 1987; Hackett and Houghton 1989; Price et al. 1999; Gamble et al. 2003; Price et al. 2012; Conway et al. 2015). The stratigraphy and chronology developed for the Mt. Ruapehu edifice shows several growth periods of lava effusion over at least the past 250,000 years (Fig. 1). Tost and Cronin (2015) used detailed chronology from dated mass-flow units exposed within distal volcaniclastic deposit sequences to establish a detailed stratigraphic framework for the pre-50 ka history of the volcano. They defined three eruptive intervals additional to those seen on the composite cone and provided evidence that extended Mt. Ruapehu's age back to >340 ka (Table 1). Presented here are the results of new petrography and whole-rock chemistry studies from clasts within the distal volcaniclastic deposit sequences surrounding Mt. Ruapehu. These data have implications for the interpretation of the long-term magmatic evolution of the composite volcano. This approach outlined here shows how petrological and geochemical study of (lithic) clasts in a succession of mass-flow deposits can be used to constrain the very earliest magmatic history of stratovolcanoes such as Mt. Ruapehu.

Geological setting

Mt. Ruapehu is a typical composite cone or stratovolcano in form and construction history (Cole 1978; Hackett and Houghton, 1989). Its broad summit hosts at least three explosive vents with the southernmost and currently active crater being filled by an acidic lake (Houghton et al. 1987). Seismic evidence (Villamor and Berryman 2006a, b; Salmon et al. 2011), and xenolith-petrology studies show that the basement beneath the volcano is ~40-km thick and comprises Mesozoic greywacke (upper to middle crust) underlain by meta-igneous rock (Graham and Hackett 1987; Graham et al. 1990; Adams et al. 2007; Price et al. 2012). Over the past 2 ka, Mt. Ruapehu's volcanic activity has been characterised by frequent small-scale eruptions (<0.05 km^3), occurring at decadal intervals, with each episode lasting for weeks to several months (e.g. Lecointre et al. 2004).

Four major cone-building episodes were identified from deposits mapped on Mt. Ruapehu (Fig. 1), including the Te Herenga Formation (250–180 ka), the Wahianoa Formation (160–115 ka), the Mangawhero Formation (55–45 ka; 30–15 ka) and the Whakapapa Formation (<15 ka) (Hackett and Houghton 1989; Gamble et al. 2003). The oldest dated lavas on Mt. Tongariro are 273 ± 22 ka, while at Mt. Ruapehu they are 230 ± 1 ka (Stipp 1968; Hobden et al. 1996).

Petrologically, the Mt. Ruapehu lava flow sequences comprise mainly plagioclase-pyroxene-phyric, plagioclase-phyric and pyroxene-(olivine)-phyric andesites, although pyroxene-phyric, olivine-pyroxene-phyric and rare hybrid andesite rock types also occur (Graham and Hackett 1987; Graham et al. 1995; Gamble et al. 2003; Price et al. 2012). Dacites are rare, and only one basalt flow was identified. The Ruapehu cone lavas become progressively more enriched in SiO_2, K_2O, Rb and Sr over time, although their geochemical compositions vary widely within each of the major eruptive episodes, with the exception of the uniform Te Herenga Formation (Fig. 2) (Gamble et al. 2003; Price et al. 2005, 2012). The temporal geochemical and petrographic variations at Mt. Ruapehu were interpreted to reflect open-system processes. A complex plumbing system is envisaged, comprising numerous small dykes and sills distributed throughout the crust and upper mantle beneath the volcano (Price et al. 1997; Gamble et al. 1999, 2003; Price et al. 2005, 2007, 2012). This is consistent with seismic anisotropy measurements, which suggest the presence of dyke-like structures <10 km beneath the edifice (Miller and Savage 2001; Gerst and Savage 2004). Stagnant melt is thought to crystallize and fractionate within small isolated pockets, assimilating surrounding wall rock, xenoliths and xenocrysts, and mingling with fresh magma derived from deeper in the system (Graham and Hackett 1987; Gamble et al. 1999; Price et al. 2005, 2012). Disequilibrium in Th and U isotopes shows that these processes have operated over tens of thousands of years prior to eruption (Price et al. 2007). The magma associated with the oldest Te Herenga Formation was interpreted to record the first stage of mantle/lower crust interaction (Price et al. 1997; Gamble et al. 1999; Price et al. 2005). The scarcity of hornblende in Mt. Ruapehu lavas was interpreted to indicate that crystallization occurred from

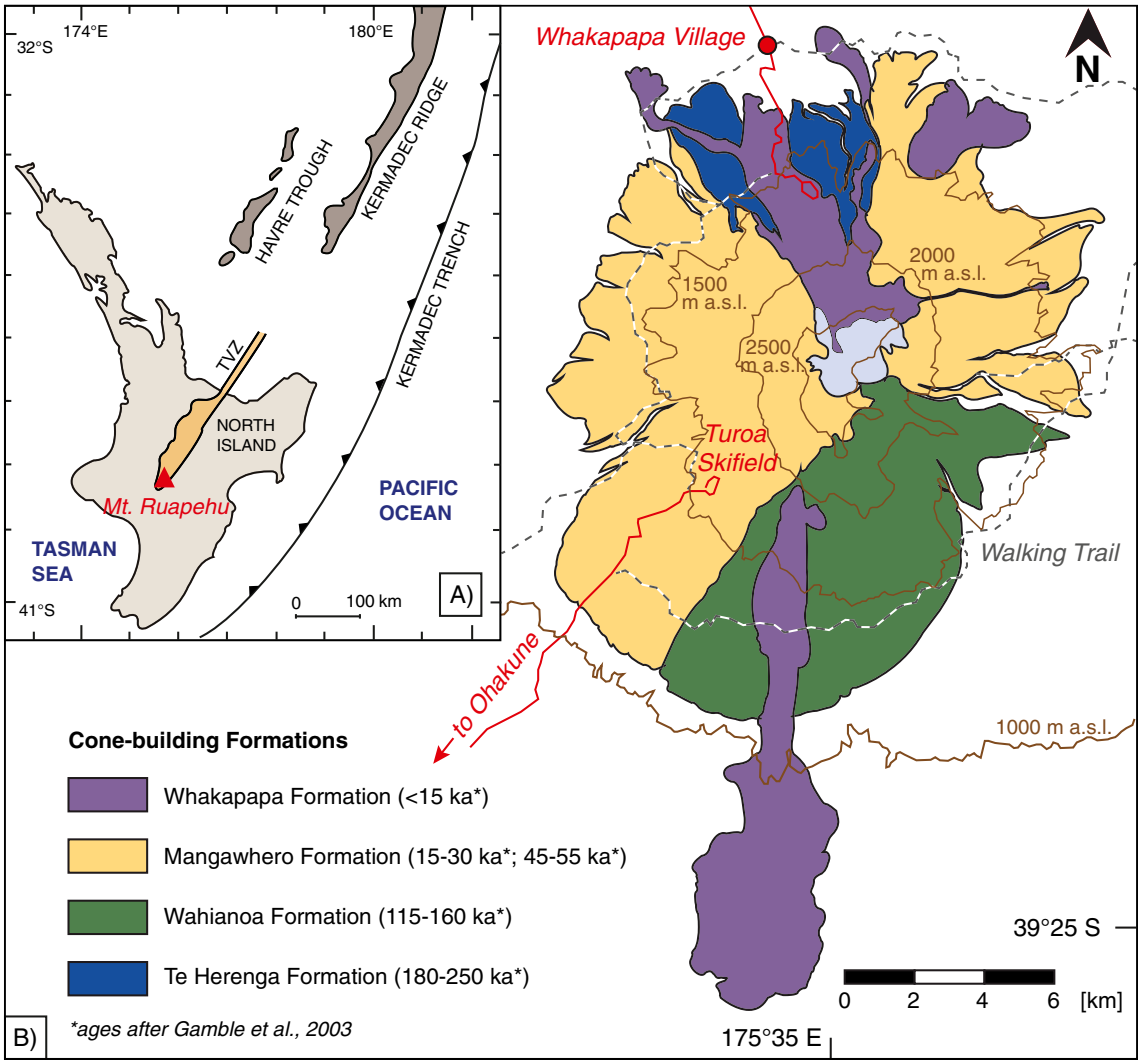

Fig. 1 The individual cone-building formations exposed on the Mt. Ruapehu edifice as mapped and identified by Hackett and Houghton (1989)

water-undersaturated melts (2–5 wt.%) (Graham et al. 1995). Petrological and geochemical studies suggest that crystallization temperatures ranged between 1200 and 1050 °C and crystallization pressures were below 10 kbar (Green and Hibberson 1969; Lindsley 1983; Graham and Hackett 1987).

Distal mass-flow deposits

Mass-flow deposit sequences from Mt. Ruapehu were emplaced between 340 and 60 ka along six major river valleys that radiate outward from the south to west flanks of the volcano (Fig. 3) (Tost et al. 2014, 2015; Tost and Cronin 2015). The deposits are from oldest to youngest: the Turakina conglomerate (Turakina River, 340–310 ka); the Mataroa Formation (Hautapu River, ~280–125 ka); the Lower Whangaehu Formation (Whangaehu River, ~230–210 ka); the Piriaka Formation (Whakapapa and Whanganui Rivers, ~200–80 ka); the Oreore Formation (Mangawhero River, ~180–160 ka); and the Pukekaha Formation (Manganuioteao River, ~90–50 ka) (Tost and Cronin 2015). With the exception of the Turakina conglomerate, the mass-flow formations comprise debris avalanche deposits (Keigler et al. 2011; Tost et al. 2014), interbedded with debris flow and hyperconcentrated flow deposits (e.g. Keigler et al. 2011; Tost and Cronin 2015). The debris avalanche deposits are poorly sorted and unbedded, with large clasts (≤4 m) supported in a sand-silt matrix (Keigler et al. 2011; Tost et al. 2014, 2015). These deposits contain dominantly lava blocks and pumice. Several units contain jigsaw-fractured angular blocks and poorly to well-rounded andesite lava fragments (66–90 % by vol.), along with hydrothermally altered clasts (≤5 % by vol.), ripped-up andesite river gravel (≤10 % by vol.) and Tertiary sediment (≤15 % by vol.). Some lahar and debris avalanche deposits contain variably weathered angular to subrounded pumice (≥20 % by vol.). The stratigraphic relationships of the ring-plain deposits with the Mt. Ruapehu cone-building lava formations are outlined in Table 1.

Table 1 The eruptive episodes of Mt. Ruapehu and correlations with the depositional ages of the mass-flow deposits sampled. *TVZ* Taupo Volcanic Zone

South Taranaki-Wanganui marine terraces[a]	Rangitikei River terraces[b]	Cone-building formation[c]	Eruptive interval[d]	River valley[d]	Associated mass-flow deposits[d]
	Aldworth (340–350 ka)				
Braemore (337 ka)					
Brunswick (309 ka)			Turakina (340–280 ka)	Turakina River	Conglomerate
				Hautapu River	Conglomerate
Ngarino (211 ka)		Te Herenga (250–180 ka)		Hautapu River and Whangaehu River	Debris avalanche Hyperconcentrated flow Debris flow Debris flow Hyperconcentrated flow Debris flow Hyperconcentrated flow
	Burnand (240–280 ka)			Whanganui River	Debris avalanche Hyperconcentrated flow Fluvial Hyperconcentrated flow Debris avalanche Hyperconcentrated flow Fluvial Debris flow Debris flow Fluvial
			Oreore (180–160 ka)	Mangawhero River	Debris avalanche Hyperconcentrated flow Conglomerate Hyperconcentrated flow
				Whanganui River	Hyperconcentrated flow Debris flow Fluvial Hyperconcentrated flow
	Marton (140–170 ka)	Wahianoa (180–119 ka)		Manganuioteao Whanganui River Hautapu River	Diamicton Debris flow Hyperconcentrated flow
Rapanui (120 ka)	Greatford (110–120 ka)		Waimarino (100–55 ka)	Manganuioteao Whanganui River Hautapu River Waikato River Whakapapa River Manganuioteao Waimarino River Mangaturuturu	Debris flow Individual sequences of debris flow and hyperconcentrated flow deposits
Hauriri (81 ka)				Manganuioteao River	Hyperconcentrated flow Tephra Hyperconcentrated flow Debris avalanche Hyperconcentrated flow
Rakaupiko (60 ka)	Porewa (70–80 ka)			Waikato River Mangawhero River	Tephra Hyperconcentrated flow
	Rata (30–50 ka)				

[a] After Pillans (1983)

[b] After Pillans (1994)

[c] After Hackett and Houghton (1989); Gamble et al. (2003)

[d] After Tost and Cronin (2015)

Analytical methods

Samples for geochemical and petrological analysis were collected from unaltered angular to subrounded lava blocks (30–200 cm diameter) and the freshest-possible angular pumice clasts (≥10 cm) at all of the mass-flow sites (Fig. 3). Polished thin sections for petrographic and electron microprobe (EMP) analysis were prepared at the University of Ballarat, Victoria, Australia. After careful selection of non-weathered samples, 103 rocks were cut and the central

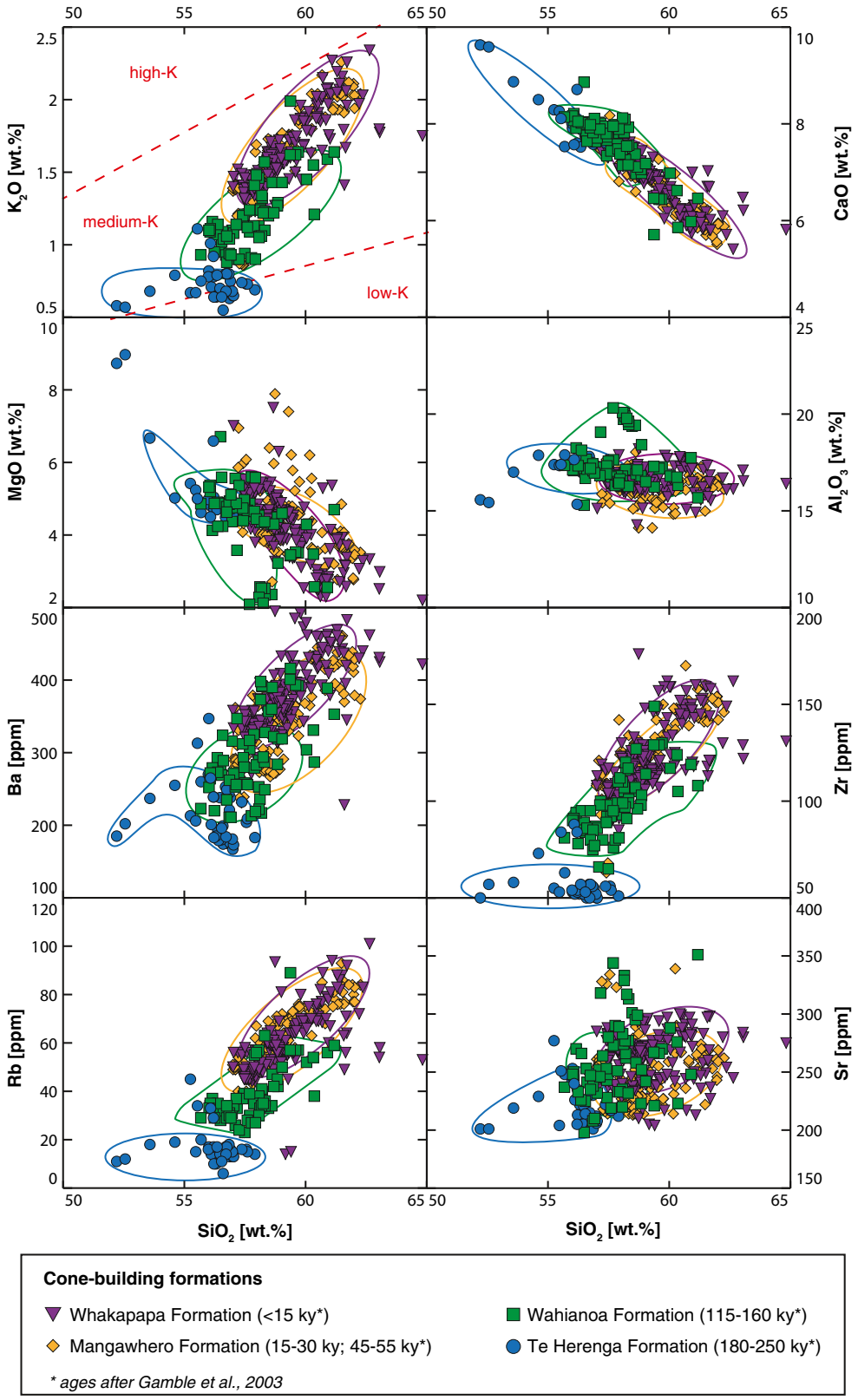

Fig. 2 SiO_2 variation diagrams for selected major components and trace elements showing variation in whole-rock compositions for individual Ruapehu cone-building formations. Labels are colour-matched to Fig. 1 and fields are drawn for the bulk composition of each formation. Normalized values have been used for major element compositions. Data from Price et al. (2012) and ages after Gamble et al. (2003). Potassium fields are after LeMaitre (1989)

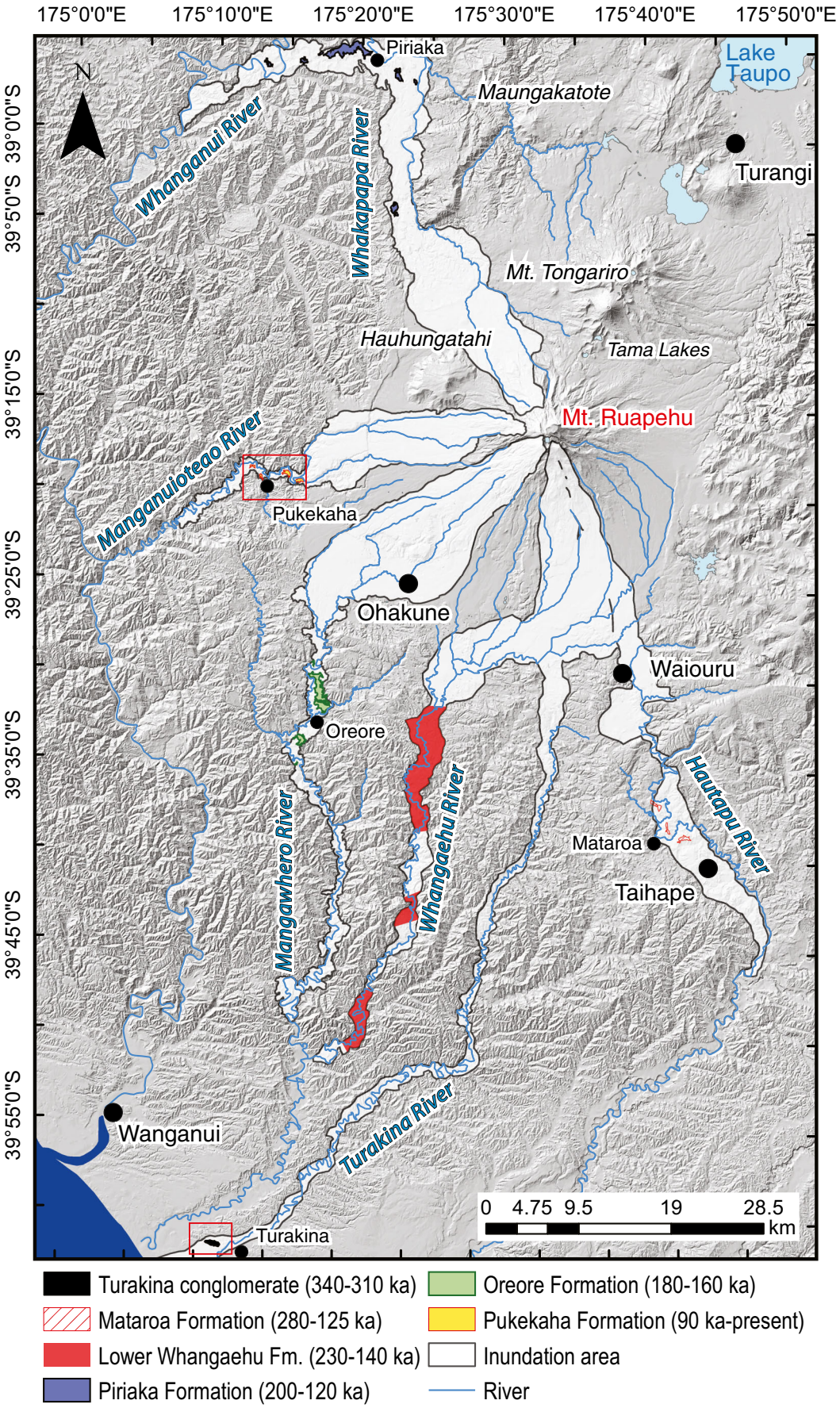
175°0'0"E
175°10'0"E
175°20'0"E
175°30'0"E
175°40'0"E
175°50'0"E
39°0'0"S
39°5'0"S
39°15'0"S
39°25'0"S
39°35'0"S
39°45'0"S
39°55'0"S
N
Piriaka
Lake Taupo
Maungakatote
Whanganui River
Whakapapa River
Turangi
Mt. Tongariro
Hauhungatahi
Tama Lakes
Mt. Ruapehu
Manganuioteao River
Pukekaha
Ohakune
Waiouru
Oreore
Mangawhero River
Whangaehu River
Hautapu River
Mataroa
Taihape
Wanganui
Turakina River
Turakina
0 4.75 9.5 19 28.5
km
Turakina conglomerate (340-310 ka)
Oreore Formation (180-160 ka)
Mataroa Formation (280-125 ka)
Pukekaha Formation (90 ka-present)
Lower Whangaehu Fm. (230-140 ka)
Inundation area
Piriaka Formation (200-120 ka)
River

◀ **Fig. 3** Digital elevation model outlining areas of initial mass-flow deposition (*yellow fields*). Exposures of the volcaniclastic rocks studied are limited to the distal Ruapehu ring plain (*red field* and *rectangles*). Map modified after Tost et al. (2014), and faults (*red lines*) after Villamor and Berryman (2006a, b)

~3 × 3 × 3 cm portions were crushed and ground in a tungsten carbide ring mill at the University of Auckland, New Zealand. Contamination of trace elements during the crushing process is limited to W and Co, while contamination of Ta and Nb is negligible (Roser et al. 2003; Martin et al. 2013).

Images of thin sections were obtained with a Nikon DS-U1 digital camera attached to a Nikon Eclipse E600 POL microscope at Massey University, Palmerston North, New Zealand.

Major (e.g. Si, Al, Mg, Fe, Ca, K and Na) and minor element concentrations (e.g. Ti, Mn, P and S) were obtained as oxide components on whole-rock samples at the University of Auckland, New Zealand, using X-ray fluorescence (XRF) and methods similar to those described by Norrish and Hutton (1969). In general, precision for each major or minor element is better than ±1 % (1σ) of the reported value (supplementary material). Using the fused glass discs prepared for XRF analysis, trace elements were measured by laser ablation inductively coupled plasma mass spectrometry (LA-ICP-MS) at the Research School of Earth Sciences, Australian National University, with an Excimer LPX120 laser (193 nm) and an Agilent 7500 mass spectrometer (Eggins et al. 1998). For trace elements, precision determined by repeated analyses of AGV-2 and BCR-2 standard rock is better than ±4 % (RSD), and the accuracy is better than 5 % at the 95 % confidence level (supplementary material).

Hornblende analyses were obtained with a JEOL JXA-840A electron microprobe (EMP) at Massey University, Palmerston North, New Zealand, using a LINK systems LZ5 detector, a QX2000 pulse processor and ZAF-4/FLS matrix correction software. Standard operating conditions include an accelerating voltage of 15 kV, a beam current of 0.5 nA, a beam diameter of 3 μm and a live count time of 100 s. Calibration was performed using a suite of Astimex™ mineral standards. The estimated precision for oxide analyses obtained by EMP is better than ±3 %.

The $^{40}Ar/^{39}Ar$-age of hornblende was obtained at the OSU Argon Geochronology Laboratory, Oregon, USA, using an ARGUS VI multi-collector mass spectrometer. The selected sample was crushed and sieved to extract grains between 200 and 300 μm in size. Hornblende separates were obtained by hand-picking. The resulting ages were calculated using the ArArCALC v2.5.2 software package (Koppers 2002), with precision being within ±2σ.

Results

Petrology

The volcanic clasts sampled from the Ruapehu mass-flow deposits range from dense lava to pumice (up to 40 % vesicles; Fig. 4a). All are porphyritic with up to 10 % phenocrysts in pumice and up to 45 % in lavas contained within fine-grained groundmass. The phenocrysts vary between 0.4 and 2.0 mm in size, with assemblages including plagioclase + orthopyroxene + clinopyroxene + titanomagnetite ± olivine ± hornblende. Inequigranular porphyritic and generally hypocrystalline textures dominate, comprising euhedral to subhedral phenocrysts within microcrystalline and hyaline groundmass (Fig. 4b, c). Glomerocrysts (Fig. 4d) are limited to samples from the Oreore (~180–160 ka) and Pukekaha Formations (~90–50 ka). Holocrystalline xenoliths, up to 2 mm across, are common within all samples (2–15 %) and comprise meta-sedimentary and meta-igneous rocks.

Phenocryst characteristics

Plagioclase is the most abundant mineral phase (60–65 % on average), forming euhedral to subhedral phenocrysts, as well as groundmass microlites (Fig. 4). Most crystals show Carlsbad and albite twinning, and oscillatory and complex zoning is common. The larger phenocrysts (>0.6 mm) are sieve-textured, with strong corrosion in the crystal cores, which are surrounded by fresh rims (Fig. 4e). In rare cases, entire plagioclase crystals show partial resorption textures. The plagioclase phenocrysts in the Turakina conglomerate samples (~340–310 ka) are the smallest (rarely exceeding 0.4 mm) and few, if any, show resorption textures (Fig. 4a).

Orthopyroxene and clinopyroxene are also ubiquitous (collectively 15–20 % on average), occurring as euhedral to subhedral phenocrysts and as groundmass microlites. Oscillatory, continuous and discontinuous zoning are common. Larger clinopyroxene phenocrysts (>0.6 mm) are commonly sieve-textured, with corrosion strongest in the crystal cores (Fig. 4b, f).

Titanomagnetite is a common mineral phase (5 % on average), occurring as euhedral to subhedral and homogenous phenocrysts and as groundmass microlites. It is also an abundant mineral inclusion within pyroxene phenocrysts, occurring mainly along cleavages and/or fractures.

Olivine is rare and, where found, does not exceed 3 %. It is most abundant in samples of the Oreore Formation (~180–160 ka) and almost entirely absent in clasts from the Mataroa (~280–125 ka), Lower Whangaehu (~230–210 ka) and Pukekaha (~90–50 ka) Formations. When present, it

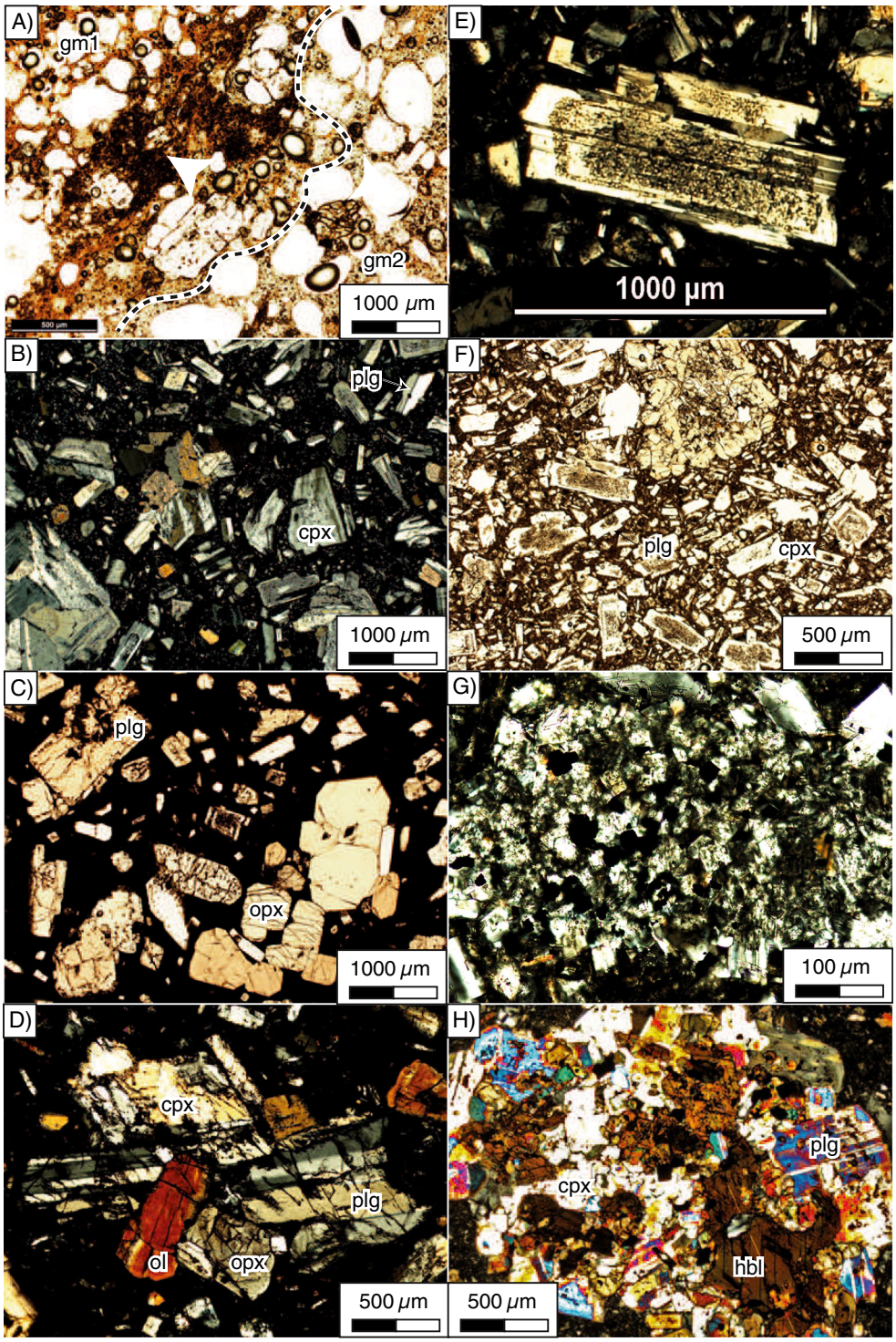

Fig. 4 Photomicrographs of clasts from the Ruapehu mass-flow deposits. **a** Plane-polarized photomicrograph of two different groundmass types. Features indicating magma mixing prior to eruption are present within the Turakina conglomerate, the Oreore Formation and the Pukekaha Formation. Pyroclasts contain up to 40 % subspherical, and in part elongated vesicles. **b** Cross-polarized photomicrograph of the typical mass-flow mineral assemblage with subhedral phenocrysts in a microcrystalline groundmass. Plane-polarized photomicrograph. **c** A hyaline groundmass is limited to samples taken from initial pyroclasts. **d** Clasts from lava flow sequences are generally porphyritic and comprise sieve-textured plagioclase and pyroxene phenocrysts. **e** Cross-polarized photomicrograph of a typical sieve-textured plagioclase phenocryst within the Ruapehu-sourced volcaniclastics. **f** Cross-polarized photomicrograph of a glomerocrysts made up of plagioclase + orthopyroxene + clinopyroxene + olivine. **g** Cross-polarized photomicrograph of a fine-grained meta-sedimentary xenolith. **h** Cross-polarized photomicrograph of a meta-igneous hornblende-bearing xenolith. *gm* groundmass, *plg* plagioclase, *cpx* clinopyroxene, *opx* orthopyroxene, *ol* olivine, *hbl* hornblende

forms small (<0.4 mm) euhedral phenocrysts or inclusions within clinopyroxene phenocrysts.

Hornblende is only present as an accessory phenocryst phase (≤1 %) in some clasts of the Lower Whangaehu Formation (~230–210 ka), occurring as small (≤0.2 mm) brown, subhedral crystals with thin outer reaction rims.

Groundmass characteristics

The groundmass is hyaline in pyroclast samples and microcrystalline in lava samples. In clasts sampled from the Mataroa (~280–125 ka), Lower Whangaehu (~230–210 ka) and Piriaka Formations (~250–80 ka), the groundmass is

homogeneous and dominantly made up of plagioclase + titanomagnetite ± pyroxene. Samples from the Turakina conglomerate, as well as the Oreore (~180–160 ka) and Pukekaha (~90–50 ka) Formations, show both microlite-rich and hyaline textures (Fig. 4g).

Autolith characteristics

Autoliths, up to 2 cm in diameter, occur only in samples from the lower Piriaka Formation (~250–180 ka). They consist of inequigranular textured hypocrystalline clasts with subhedral phenocrysts in a microcrystalline groundmass. The autolith groundmass generally contains more microlites than the surrounding material. The major phenocryst and microlite mineral assemblage includes plagioclase + clinopyroxene + orthopyroxene + titanomagnetite. The phenocrysts show strong marginal resorption, including alteration of rims and partial marginal fusion, as well as strongly altered phenocrysts.

Xenolith and xenocryst characteristics

Xenoliths embedded within the volcanic clasts are small (up to 2 mm) and include one meta-sedimentary and two distinct meta-igneous types. The meta-sedimentary xenoliths are fine-grained and composed of granulitic quartz + granoblastic plagioclase + orthopyroxene + magnetite (Fig. 4g). They occur in samples of all mass-flow unit suites with the exception of those from the Turakina conglomerate (~340–310 ka). The meta-igneous xenoliths are ubiquitous and generally coarser grained than the meta-sedimentary types. They contain granoblastic plagioclase + orthopyroxene + olivine + clinopyroxene + titanomagnetite (cf., Graham et al. 1990; Graham et al. 1990; Price et al. 2012). A second type of meta-igneous xenolith that occurs only in the Turakina mass-flow deposit contains hornblende, which is commonly mantled by clinopyroxene, along with plagioclase + orthopyroxene + olivine + clinopyroxene + titanomagnetite (see above). Furthermore, hornblende occurs in some lava clasts from the Turakina deposit as up to 2-mm-long subhedral xenocrysts (Fig. 4h), some of which show discontinuous zoning and varying degrees of resorption, ranging from reaction rims to complete replacement by opaque phases. Hornblende is extremely rare in younger Ruapehu eruptives and in the xenoliths they contain (Graham and Hackett 1987; Price et al. 2012).

Amphibole mineral chemistry

Amphibole compositions from meta-igneous xenoliths found in the Turakina conglomerate (~340–310 ka) are shown in Table 2. All are pargasite (after Leake et al. 1997, classification) and show only slight core to rim compositional changes. One amphibole was dated by the $^{40}Ar/^{39}Ar$ method and the plateau age obtained is 486.5 ± 37.6 ka, which is the oldest age so far obtained from any Ruapehu eruptive (Fig. 5).

Geochemistry

In the lava and the freshest angular pumice clasts sampled from the mass-flow sequences, the abundances of incompatible major and minor elements (e.g. Si, K, Na) and trace elements (e.g. Rb, Zr, Rare Earth Elements) vary systematically, apparently reflecting distinctive magmatic cycles (Table 3; complete data for all suites is provided in the supplementary material). The overall suite is subalkaline and ranges from basalt to andesite (50.9 to 59.6 wt.% SiO_2 and 3.1 to 5.1 wt.% total alkalis) (Fig. 6; LeBas et al. 1986). The clasts from the Turakina conglomerate (~340–310 ka) are exclusively andesite. The only two basaltic clasts are from the Oreore Formation (180–160 ka), which comprises a suite dominated by basaltic andesite with less common andesite. The samples taken from the other mass-flow formations are dominantly andesite with minor basaltic andesite.

Major element composition

Silica-variation diagrams for selected normalized (to 100 % by weight) major elements are illustrated in Fig. 7. Generally, the whole-rock silica content of the distal volcaniclastic rocks is lower than that from the lava flow sequences exposed on the flanks of Mt. Ruapehu (Fig. 2). Samples of the Turakina conglomerate (~340–310 ka) plot at the more evolved end of the overall suite, with normalized SiO_2-contents generally exceeding 58 wt.%. Most of the samples from Lower Whangaehu (~230–210 ka), Mataroa (~280–125 ka), Piriaka (~250–80 ka) and Pukekaha (~90–50 ka) Formations have normalized SiO_2 contents ranging between 56 and 58 wt.%. Within each formation of stacked mass-flow deposits (Tost and Cronin 2015), the rocks with the lowest silica contents usually correspond to the stratigraphically oldest (basal) flow units, with highest values occurring in the youngest (top) mass-flow units.

The normalized potassium contents of most mass-flow sequences are similar to those observed in the Wahianoa Formation on the edifice (Fig. 2) (160–119 ka; Gamble et al. 2003). Low K_2O contents, similar to those of the Te Herenga Formation (Fig. 2) (250–180 ka; Gamble et al. 2003), occur in the Oreore Formation debris avalanche deposits (~180–160 ka). In the Pukekaha Formation (~90–50 ka), K_2O content decreases upwards through the mass-flow sequence from 1.91 to 1.13 wt.%.

The normalized CaO and MgO contents show a reverse correlation with normalized SiO_2 abundance (Fig. 7), as has

Table 2 Representative major and trace element concentrations of lava and fresh pumice samples from the Ruapehu mass-flow deposits sampled here. A complete database is included in the supplementary material

Sample Label	RAT-03 hbl1_core	RAT-03 hbl1_rim	RAT-03 hbl2_rim	RAT-03 hbl2_core	RAT-03 hbl3_rim	RAT-03 hbl3_core	RAT-03 hbl4_rim	RAT-03 hbl4_core	MAN-KL7 hbl1_core	MAN-KL7 hbl1_rim	MAN-KL7 hbl2_rim	MAN-KL7 hbl2_core	MAN-KL7 hbl3_rim
SiO_2 (wt.%)	42.93	42.95	43.03	43.03	42.49	42.90	43.10	42.90	42.90	42.72	43.69	42.89	43.54
TiO_2 (wt.%)	2.03	2.00	1.67	1.67	1.94	1.82	2.03	1.82	1.20	1.23	1.26	1.28	1.10
Al_2O_3 (wt.%)	10.65	10.64	11.45	11.45	11.34	11.14	10.84	11.14	11.65	12.01	10.70	11.54	11.10
Cr_2O_3 (wt.%)	0.11	0.06	0.07	0.07	0.12	0.04	0.05	0.04	0.11	0.10	0.09	0.06	0.16
FeO (wt.%)	15.25	15.24	14.57	14.57	13.92	14.57	14.07	14.57	14.32	14.65	14.87	14.97	14.43
MnO (wt.%)	0.26	0.35	0.38	0.38	0.29	0.34	0.28	0.34	0.31	0.40	0.36	0.43	0.35
MgO (wt.%)	12.50	12.55	12.86	12.86	13.16	13.07	13.16	13.07	13.07	12.88	12.99	12.57	13.20
CaO (wt.%)	10.95	10.95	11.08	11.08	11.09	11.11	11.23	11.11	11.03	10.88	11.05	11.04	10.99
Na_2O (wt.%)	2.04	2.00	2.12	2.12	2.13	2.19	2.04	2.19	2.03	2.03	1.91	1.94	1.92
K_2O (wt.%)	0.37	0.35	0.31	0.31	0.35	0.33	0.34	0.33	0.29	0.33	0.28	0.31	0.29
F (wt.%)	0.00	0.00	0.00	0.00	0.00	0.00	0.00	0.00	0.00	0.00	0.00	0.00	0.00
Cl (wt.%)	0.12	0.13	0.09	0.09	0.07	0.07	0.07	0.07	0.07	0.05	0.05	0.08	0.08

Sample Label	MAN-KL7 hbl3_core	MAN-KL7 hbl4_rim	MAN-KL7 hbl4_core	MAN-OH4 hbl1_core	MAN-OH4 hbl1_rim	MAN-OH4 hbl2_rim	MAN-OH4 hbl2_core	MAN-OH4 hbl3_rim	MAN-OH4 hbl3_core	MAN-OH4 hbl4_rim	MAN-OH4 hbl4_core
SiO_2 (wt.%)	42.65	43.58	42.86	42.93	42.58	43.00	43.34	43.25	41.79	43.52	42.85
TiO_2 (wt.%)	1.29	1.23	1.31	1.21	1.23	1.27	1.24	1.35	1.35	1.26	1.16
Al_2O_3 (wt.%)	11.77	10.98	11.42	10.86	11.75	11.19	11.12	11.07	13.03	10.73	11.91
Cr_2O_3 (wt.%)	0.07	0.09	0.01	0.05	0.13	0.15	0.08	0.17	0.15	0.06	0.18
FeO (wt.%)	15.01	14.58	14.83	14.97	15.68	14.50	14.40	14.94	14.20	14.59	14.82
MnO (wt.%)	0.31	0.33	0.39	0.45	0.38	0.31	0.27	0.36	0.26	0.42	0.40
MgO (wt.%)	12.61	13.21	12.83	12.57	12.27	12.86	13.12	12.74	12.82	13.02	12.74
CaO (wt.%)	10.78	10.98	11.09	10.88	10.85	11.05	11.06	10.99	10.98	11.02	10.97
Na_2O (wt.%)	2.03	1.95	2.39	1.90	2.05	1.95	1.91	1.85	2.12	1.86	1.93
K_2O (wt.%)	0.34	0.29	0.29	0.29	0.33	0.29	0.29	0.32	0.34	0.28	0.32
F (wt.%)	0.00	0.00	0.00	0.00	0.00	0.00	0.00	0.00	0.00	0.00	0.00
Cl (wt.%)	0.13	0.10	0.06	0.09	0.10	0.08	0.10	0.09	0.09	0.07	0.07

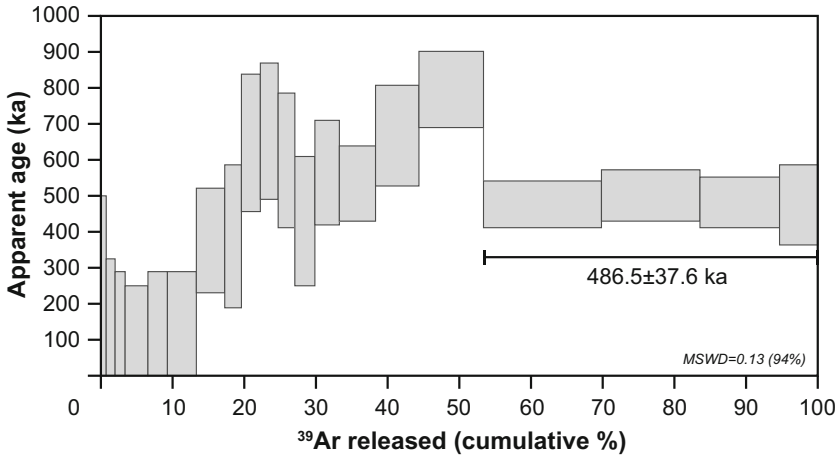

Fig. 5 Results of the $^{40}Ar/^{39}Ar$ step-heating of the hornblende xenocryst within the deposits of the Turakina eruptive episode. The calibration standard used for the analyses is sanidine from the Fish Canyon Tuff, Colorado, USA (FCT-NM), dated at 28.02 ± 0.571 Ma (Renne et al. 1998)

been found for the edifice lavas (Fig. 2), with phenocryst-poor samples having the highest CaO contents. Variation in normalized Al_2O_3-contents is low (14.7–20.2 wt.%), with the concentration decreasing with decreasing age. In the oldest unit (Turakina ~340–310 ka), intermediate Al_2O_3 concentrations are found.

Trace element compositions

Systematic variations in trace element concentration reflect the evolution of a magmatic system (e.g. Wager and Mitchell 1951; Nockolds and Allen 1954). All samples of the Ruapehu mass-flow suite (Figs. 8, 9 and 10) have similar normal mid ocean ridge basalt (N-MORB)-normalized rare earth element (REE) patterns and exhibit the trace element characteristics of magmas from subduction zone settings (cf., McCulloch and Gamble 1991; Hawkesworth et al. 1993; Keleman et al. 2005) or continental crust (Weaver and Tarney 1984; Rudnick and Gao 2005). Caesium, Rb, Ba, Th, K and U are enriched relative to the light REEs (LREEs), and heavy REEs (HREEs) are depleted compared with LREE and N-MORB abundances. Rubidium is depleted relative to Cs, and Nb is depleted relative to K and La (Fig. 8). Titanium is depleted relative to elements of similar compatibility (Fig. 8), and chondrite-normalized REE patterns are characterised by distinctive negative EU anomalies (Fig. 9). The bulk of the mass-flow deposits display trace element compositions similar to those of the Te Herenga (250–180 ka; Gamble et al. 2003) and Wahianoa (160–119 ka; Gamble et al. 2003) cone-building formations on the Ruapehu edifice (Fig. 2). The Ba, Zr, Rb and Sr contents of all mass-flow samples cover a similar range and vary widely within each mass-flow suite. An exception is the Rb content within the Pukekaha Formation (~90–50 ka), which follows the same pattern as that described for the K_2O content (see above).

Discussion

Petrological and geochemical data from volcanic clasts, ~340–55 ka in age, obtained from mass-flow sequences exposed up to 90 km from Mt. Ruapehu provide new information about the ancient eruptive history of this stratovolcano. The lava flow sequences exposed on the Ruapehu edifice were previously grouped into four major cone-building episodes (Fig. 1). Six long-runout mass-flow sequences, which were recently identified, described and dated, represent eruptive intervals that overlap with the previously studied cone-building formations (Tost and Cronin 2015). There are similarities in geochemical composition and petrography between the lavas of the edifice and the igneous clasts from the distal mass-flow deposits (Figs. 7, 8, 9 and 10). These include similar LIL (large-ion lithophile) element contents (e.g. K, Rb, Sr, Ba), as well as low Nb relative to K abundances. These characteristics are generally interpreted to reflect slab fluid input (Arculus and Powell 1986; Tatsumi et al. 1986; McCulloch and Gamble 1991; Hawkesworth et al. 1993), and/or interaction between crust and mantle-derived magma (Graham and Hackett 1987; Graham et al. 1995; Price et al. 2005, 2012). The negative Ti anomaly most likely arises from fractional crystallization involving titanomagnetite or assimilation of continental crust. The slight negative Eu anomaly could reflect either fractional crystallization of plagioclase (Graham and Hackett 1987), or retention of this mineral as a restite phase during crustal anatexis (Price et al. 2012). The porphyritic basalts and andesites typically contain strongly zoned and sieve-textured pyroxene and plagioclase phenocrysts, which were at some stage not in equilibrium with the host melt. Furthermore, in all mass-flow sequences, variations of major and minor element concentrations are observed. Thus, as has been proposed for the edifice lava flow sequences, the Ruapehu rock suite as a whole reflects open-system batch-melting and/or assimilation fractional crystallization processes where repeated cycles of magma replenishment occurred within a complex crustal storage system (e.g. Price et al.

Table 3 Hornblende compositions for the meta-igneous xenoliths within the samples of the Turakina mass-flow deposit. Representative mass-flow whole-rock analyses of Ruapehu (XRF and ICP-MS combined)

Formation	1.00	2.00	3.00	4.00	5.00	6.00	7.00	8.00	9.00	10.00	11.00	12.00	13.00	14.00	15.00	16.00	17.00	18.00	19.00	20.00	21.00	22.00	23.00	24.00
	Mataroa Formation				Whangaehu Formation				Oreore Formation				Piriaka Formation				Pukekaha Formation				Turakina Formation			
Sample no.:	GW3b	GW3gr	MF3b	JW2b	MP3	MP4	TF2	TF8	KL5	KL6	KL8	KL9	PI3	PI4	PL2	KA1	RB2	RB5	MA1	MA3	TUR_01	RAT_01	RAT_02	RAT_03
SiO_2	58.53	58.70	58.71	58.72	57.64	57.64	57.79	57.42	53.52	53.64	52.53	52.93	57.30	57.53	57.28	57.52	58.16	57.91	57.97	57.95	58.65	58.65	56.91	59.31
TiO_2	0.60	0.65	0.73	0.58	0.75	0.64	0.60	0.63	0.64	0.69	0.64	0.64	0.62	0.55	0.58	0.64	0.77	0.72	0.72	0.74	0.64	0.49	0.53	0.49
$Al2O_3$	19.25	17.56	17.90	17.22	17.64	19.24	16.30	17.62	18.59	18.26	17.04	17.29	17.43	17.55	16.85	17.35	16.72	14.74	15.20	14.85	17.91	17.77	17.51	16.47
Fe_2O_3	5.78	6.87	6.95	7.06	7.82	6.68	7.67	8.01	9.63	8.88	8.36	8.42	7.88	8.28	7.89	8.07	6.79	7.26	7.27	7.23	6.80	7.00	7.30	6.69
MnO	0.09	0.11	0.11	0.13	0.12	0.10	0.13	0.13	0.15	0.14	0.14	0.13	0.12	0.13	0.13	0.12	0.10	0.11	0.12	0.11	0.11	0.12	0.11	0.11
MgO	2.08	3.73	2.91	3.91	3.54	2.74	4.75	4.15	4.98	5.48	6.26	6.32	4.37	4.16	4.97	4.21	4.19	6.95	6.17	6.63	3.36	3.05	4.22	4.13
CaO	7.33	7.16	5.97	7.06	6.95	7.83	7.27	7.46	7.67	7.92	8.15	8.14	7.41	7.66	7.76	7.02	6.86	7.16	7.50	7.33	7.15	6.67	7.47	6.89
Na_2O	3.70	3.58	3.49	3.29	3.31	3.67	3.05	3.36	2.91	2.77	3.11	3.08	3.37	3.37	3.25	3.42	3.32	2.98	3.03	3.01	3.49	3.45	3.23	3.48
K2O	1.21	1.10	1.47	1.09	1.38	1.07	1.38	1.07	0.29	0.68	0.62	0.58	1.03	0.64	0.93	1.04	1.78	1.62	1.60	1.60	1.07	0.81	0.77	0.88
P_2O_5	0.12	0.11	0.12	0.10	0.12	0.13	0.11	0.11	0.08	0.08	0.06	0.06	0.11	0.08	0.11	0.11	0.16	0.14	0.14	0.14	0.11	0.10	0.09	0.10
H_2O	0.26	0.12	0.74	0.19	0.32	0.21	0.25	0.12	0.43	0.44	1.22	0.84	0.20	0.15	0.16	0.31	0.40	0.08	0.12	0.19	0.17	0.34	0.44	0.27
LOI	0.94	0.20	0.78	0.58	0.30	−0.06	0.58	−0.20	1.03	0.90	1.76	1.44	0.06	−0.20	−0.02	0.07	0.63	0.16	0.02	0.04	0.43	1.47	1.31	1.08
Total	99.89	99.88	99.88	99.91	99.88	99.88	99.87	99.89	99.90	99.88	99.89	99.87	99.90	99.91	99.88	99.89	99.87	99.85	99.85	99.84	99.88	99.91	99.88	99.90
Be	0.84	0.85		0.92																				
Cs	1.65	1.46	2.76	1.79	2.08	1.02	2.36	1.10	0.49	1.50	1.25	1.04	1.43	0.34	1.24	1.01	3.59	3.56	2.31	3.13	1.75	1.60	1.43	1.32
Ba	309	273	402	282	299	338	335	292	236	282	235	260	264	200	283	260	349	319	337	328	296	234	247	276
Rb	30	29	48	30	39	25	39	30	4	19	16	14	26	14	24	28	61	58	54	55	31	25	22	22
Sr	261	229	253	221	266	310	267	253	218	267	257	251	250	219	249	236	261	218	248	233	265	212	243	247
Pb	7.97	7.97	68.20	8.06	10.53	8.58	13.41	31.47	52.54	36.75	28.55	28.66	24.86	31.45	25.56	5.71	9.44	8.60	8.17	8.50	14.31	23.58	32.63	39.54
Th	2.75	2.77	5.53	2.95	4.43	3.39	4.28	3.20	1.84	4.28	3.41	3.43	2.57	1.25	2.29	2.39	5.94	5.41	5.28	5.14	3.19	2.05	2.31	1.78
U	0.85	0.83	1.33	0.89	0.98	0.78	1.08	0.83	0.39	0.85	0.87	0.91	0.68	0.41	0.64	0.73	1.61	1.53	1.47	1.46	0.79	0.62	0.63	0.58
Zr	72	73	126	74	102	80	94	82	64	96	85	84	74	52	70	70	128	114	115	115	86	68	72	65
Nb	3.22	3.39	4.94	3.30	4.14	2.89	3.45	2.98	2.15	3.97	3.23	3.23	2.67	1.60	2.22	2.41	4.67	4.10	4.07	4.05	3.47	2.80	2.65	2.12
Hf	2.00	2.04	3.38	2.08	2.80	2.16	2.54	2.23	1.81	2.67	2.41	2.34	2.14	1.52	1.87	1.96	3.45	3.17	3.12	3.19	2.38	1.88	1.95	1.80
Ta	0.31	0.34	0.41	0.44	0.33	0.21	0.29	0.24	0.17	0.31	0.24	0.26	0.21	0.11	0.18	0.17	0.35	0.32	0.31	0.32	0.29	0.19	0.21	0.15
Y	14	14	20	15	20	17	18	18	16	18	19	16	17	14	16	18	18	17	17	16	16	15	13	13
Sc	16.3	20.4	23.7	23.9	29.3	21.2	30.9	27.8	35.6	34.8	33.2	33.7	27.0	28.1	28.8	25.1	20.9	25.3	27.3	26.1	23.1	20.3	26.9	24.0
V	154	181	188	179	237	193	205	209	252	222	193	194	201	205	197	200	181	188	195	197	178	147	174	164
Cr	20	88	39	66	18	35	91	62	48	108	210	218	73	44	127	76	88	334	237	309	85	23	142	126
Co	58	42	73	95	42	40	48	50	41	54	76	62	46	41	43	47	63	63	43	40	57	39	67	51
Ni	15	35	27	23	11	20	29	23	25	35	65	59	50	27	42	36	51	125	86	105	33	20	63	51
Cu	31	35	28	28	18	41	21	32	48	41	45	40	35	67	51	46	41	54	45	78	34	27	30	32
Zn	72	77	182	90	88	76	97	237	177	180	168	164	177	236	178	64	54	51	53	54	173	191	203	233
Ga	17	17	18	16	18	18	17	17	17	18	17	17	17	16	17	16	17	15	15	15	17	16	17	15
La	8.18	7.73	12.71	7.99	11.12	10.27	11.55	9.02	4.84	11.13	8.77	8.25	7.30	4.11	7.00	7.26	13.23	11.60	10.93	11.21	8.53	6.11	6.21	5.86
Ce	17.79	17.50	27.57	16.99	22.58	19.96	20.96	17.94	11.43	23.54	20.27	20.49	15.81	9.04	14.84	15.12	28.66	24.74	23.59	24.46	18.49	12.53	13.22	12.57
Pr	2.14	2.04	3.27	2.09	2.81	2.63	2.71	2.34	1.77	3.09	2.47	2.45	1.97	1.23	1.96	2.09	3.48	2.97	2.90	2.94	2.28	1.63	1.62	1.61
Nd	9.50	9.06	14.38	9.07	12.38	11.71	11.64	10.39	8.61	13.76	11.25	10.82	9.40	6.04	9.25	9.59	14.86	13.03	12.43	12.77	9.95	7.38	7.45	7.22
Sm	2.45	2.32	3.54	2.39	3.12	2.78	2.82	2.65	2.49	3.35	2.89	2.73	2.52	1.73	2.53	2.52	3.34	3.15	2.95	2.93	2.51	1.98	1.93	1.94
Eu	0.74	0.70	0.90	0.69	0.86	0.89	0.79	0.81	0.85	0.92	0.78	0.82	0.73	0.58	0.76	0.77	0.83	0.72	0.79	0.75	0.74	0.64	0.64	0.65
Gd	2.34	2.25	3.45	2.43	3.15	2.82	3.00	2.67	2.68	3.20	2.88	2.86	2.60	2.07	2.59	2.68	3.20	3.00	2.86	2.82	2.57	2.18	2.10	1.99
Tb	0.39	0.38	0.58	0.39	0.54	0.49	0.50	0.49	0.47	0.57	0.53	2.05	0.46	0.37	0.41	0.48	0.51	0.49	0.49	0.47	0.46	0.38	0.39	0.34
Dy	2.52	2.46	3.69	2.59	3.70	3.24	3.21	3.18	3.19	3.64	3.31	3.29	2.94	2.50	2.79	2.88	3.25	3.06	3.09	2.97	2.91	2.60	2.39	2.20
Ho	0.53	0.55	0.74	0.56	0.77	0.68	0.68	0.69	0.65	0.76	0.74	0.69	0.62	0.53	0.61	0.63	0.64	0.61	0.62	0.60	0.63	0.60	0.51	0.48

Table 3 (continued)

Formation	1.00 Mataroa Formation	2.00	3.00	4.00	5.00 Whangaehu Formation	6.00	7.00	8.00	9.00 Oreore Formation	10.00	11.00	12.00	13.00 Piriaka Formation	14.00	15.00	16.00	17.00 Pukekaha Formation	18.00	19.00	20.00	21.00 Turakina Formation	22.00	23.00	24.00
Er	1.53	1.60	2.20	1.76	2.20	1.91	1.96	1.99	1.99	2.23	2.19	2.08	1.88	1.56	1.76	1.89	1.92	1.86	1.84	1.70	1.86	1.74	1.55	1.42
Tm	0.25	0.25	0.33	0.27	0.33	0.31	0.32	0.30	0.28	0.33	0.33	0.31	0.28	0.24	0.27	0.28	0.30	0.26	0.27	0.25	0.29	0.29	0.24	0.22
Yb	1.65	1.62	2.25	1.77	2.10	1.90	1.97	2.06	1.96	2.24	2.19	2.06	1.90	1.66	1.77	1.91	1.95	1.81	1.74	1.70	1.87	1.96	1.55	1.53
Lu	0.27	0.25	0.33	0.26	0.33	0.29	0.30	0.32	0.30	0.32	0.32	0.30	0.29	0.25	0.27	0.29	0.28	0.27	0.26	0.26	0.28	0.31	0.24	0.23

2007, 2012). The progressive temporal shift of the mass-flow igneous clast sample suite towards more primitive compositions between ~340 and 160 ka suggests replenishment by mantle-derived basaltic melts of the mid- to upper crustal Ruapehu storage system, or increased shielding of the late stage magma from the country wall rock. Similar conclusions have been drawn to explain the development of the nearby Mt. Taranaki magmatic system, which is located c. 130 km west of Mt. Ruapehu (Turner et al. 2008, 2011).

FC-AFC-FCA and mixing modelling

In order to determine whether the major petrological processes involved in the evolution of the magmas represented by the new mass-flow samples, their compatible trace element compositions were examined in relation to FC-AFC-FCA processes (fractional crystallization—assimilation fractional crystallization—fractional crystallization assimilation). This was done using a mixing modeler developed by Ersoy and Helvaci (2010) (Fig. 11). The relative ratio of assimilated material to crystallized material (r) and the "increments" value were chosen on the basis of arguments made by Graham and Hackett (1987), who postulated that the Ruapehu magmas were most likely generated from primitive mantle-derived melts subjected to 30 % crystal fractionation and 6 % crustal assimilation. Assuming constant decompression and cooling of the andesitic Ruapehu melts with an initial temperature of 1050–1200 °C (Green and Hibberson 1969; Lindsley 1983; Graham and Hackett 1987) and an approximate water content of 2–5 wt.% (Graham et al. 1995; Price et al. 2012), gradual fractional crystallization would result in a phenocryst growth succession of orthopyroxene ≥ plagioclase > titanomagnetite > clinopyroxene (Moore and Carmichael 1998). In the case of basaltic andesitic melt compositions, as observed in the clasts of the Oreore eruptive episode and the Te Herenga cone-building formation, the crystallization succession changes to olivine > clinopyroxene + plagioclase > orthopyroxene (Moore and Carmichael 1998). These results are in consistency with the observed petrology of the andesitic clasts exposed within the mass-flow deposits.

The mass-flow samples indicate an evolution controlled by decoupled assimilation and fractional crystallization processes (FCA), accompanied by magma mixing. Thus, wall-rock assimilation dominated over fractional crystallization during magma storage in the middle to upper continental crust. Magma mixing is likely to have been more important than previously assumed by Graham and Hackett (1987), especially during the Turakina eruptive episode (340–280 ka; Tost and Cronin 2015). The strongly sieve-textured plagioclase and pyroxene phenocrysts are also an indication of disequilibrium crystallization, which could arise from the injection of new magma into the storage systems (Fig. 4e). These features can be interpreted to show that a long-lived (>340–280 ka),

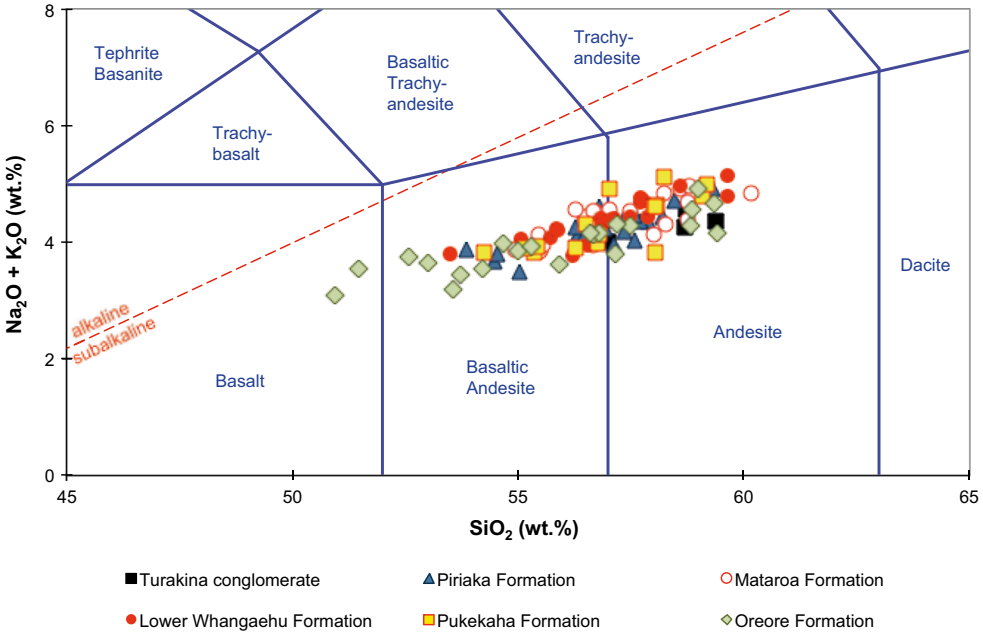

Fig. 6 Total alkali vs. silica classification for clasts from the Ruapehu mass flows. Normalized values have been used for major element compositions. Nomenclature after LeBas et al. (1986)

primitive (≤50 wt.% SiO_2), deep (~40 km; Villamor and Berryman, 2006a) magma-storage system existed from very early in Ruapehu's history, with smaller individual high-level magma reservoirs being repeatedly recharged from the deeper levels of the storage system (as also described by Graham and Hackett 1987; Price et al. 2005). The dominant magma-modification process within each mass-flow suite appears to have been related to shifts from magma mixing to FCA processes, which may indicate cycles from low to high mantle-magma supply rates.

The Turakina eruptive epoch (340–280 ka; Tost and Cronin 2015)

The mass-flow deposit exposed at Turakina, approximately 90 km south-southwest of Mt. Ruapehu (Fig. 3), has a well-constrained depositional interval between 340 and 310 ka (Tost and Cronin 2015). This makes it the oldest known sample suite from Mt. Ruapehu, around 90 ka earlier than the lavas of the oldest Te Herenga cone-building formation (250–180 ka; Gamble et al. 2003). The andesite clasts in the Turakina deposit contain two contrasting types of groundmass, indicating magma mingling (Fig. 4f). Mixing and mingling of magmas prior to eruption is also consistent with the major and trace element variations observed. The trace element behaviour of the Turakina samples contrasts with that observed in the younger rock suites (Fig. 10). Despite the comparatively high SiO_2 contents, concentrations of K, Rb and Zr are among the lowest determined within the Ruapehu mass-flow suite (Fig. 7). Neither Rayleigh fractionation nor crustal assimilation models can adequately explain this geochemical signature. At the time the Turakina formation was emplaced, major rhyolitic caldera-forming eruptions occurred in the Taupo Volcanic Zone (TVZ), producing numerous ignimbrites (Houghton et al. 1995). The regional thermal conditions required to generate these large-scale silicic magmatic systems may have also affected the lithosphere beneath Mt. Ruapehu, causing more extensive crustal melting and/or assimilation, which may explain the elevated silica content of the Turakina andesites. The Turakina suite has small phenocrysts (≤0.4 mm), suggesting rapid magma ascent. The variable major and trace element concentrations of the Turakina samples indicate autonomous differentiation of mantle-derived melts within small-scale crustal storage systems prior to infusion of new magma and eventual eruption (as per the model of Price et al. 2005, 2007, 2012).

The data for the Turakina conglomerate provide new insights into how the early Mt. Ruapehu magma system developed. The meta-igneous xenoliths are amphibole-bearing, and a number of the lava clasts contain ≤2-mm-long pargasite xenocrysts. As already noted, amphibole is extremely rare in the Ruapehu cone lavas (Graham and Hackett 1987; Palmer and Neall 1989; Price et al. 2012). Hornblende is also rare in the Tongariro Volcanic Centre (TgVC), where it is limited to a lava flow in the Tama Lakes area and another on the Maungakatote satellite cone (Fig. 3) (Cole et al. 1983). The gabbroic mineral assemblage of the meta-igneous xenoliths may support previous suggestions for an oceanic substrate underlying the North Island meta-greywacke basement (e.g. Graham et al. 1990; Price et al. 2005, 2012), and their radiometric age, petrology and geochemistry are consistent with the hypothesis that inception of Ruapehu volcanism was preceded c. 500 ka ago by underplating of the crust by mantle-

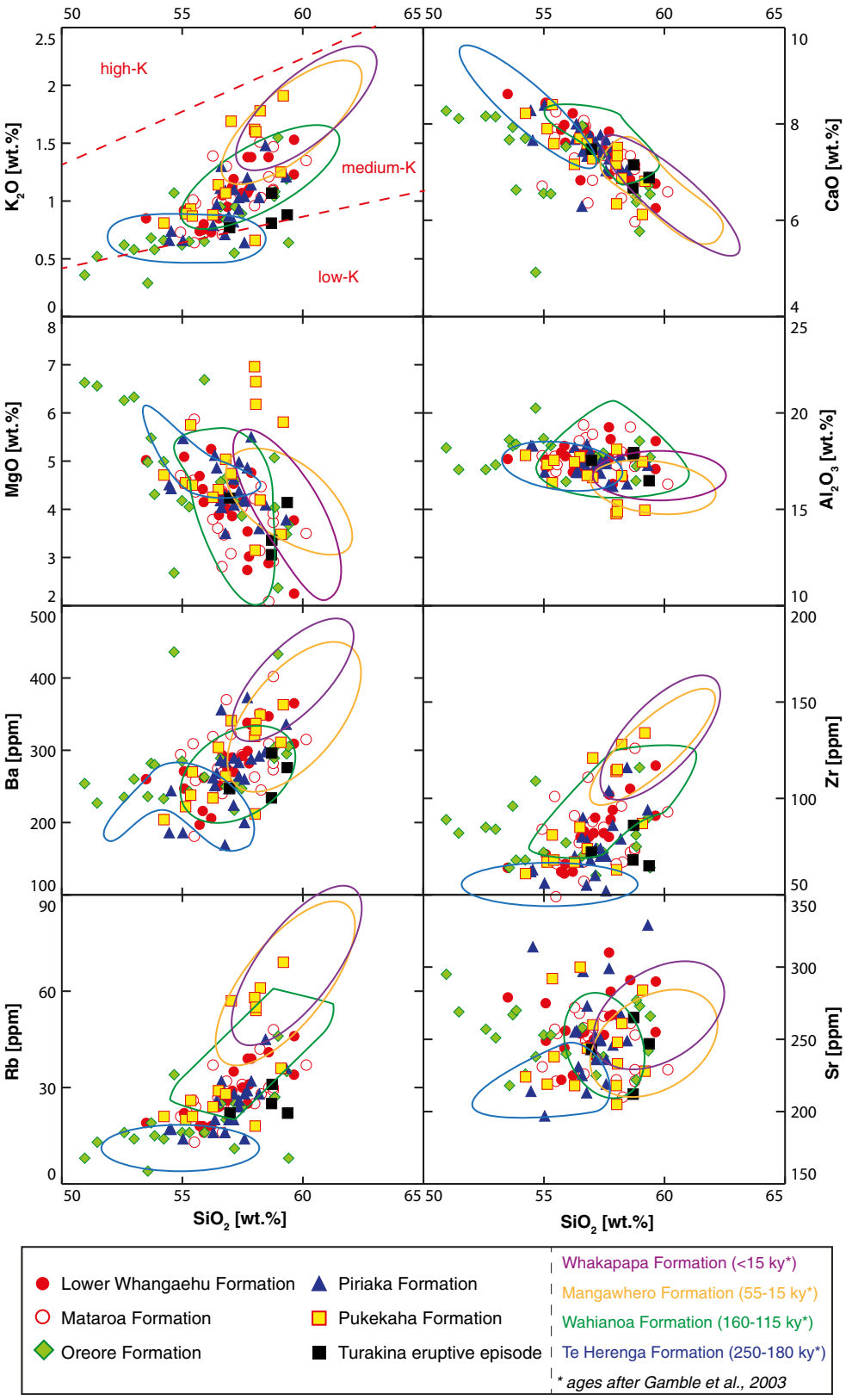

Fig. 7 Selected representative major and trace element variation diagrams for lava and pumice clasts from the Ruapehu mass flow deposits. Values normalized to 100 % have been used for major element compositions. Fields drawn for lava flow formations correspond to those shown in Fig. 2. Potassium fields after LeMaitre (1989)

derived melts (e.g. Stern et al. 2010; Price et al. 2012). Davidson et al. (2007) suggest that mid- to deep-crust amphibole fractionation is very common at arc volcanoes, even in cases where amphibole phenocrysts are absent. However, in the case of the Mt. Ruapehu mass-flow samples, trace element ratios of Dy/Yb and La/Yb indicate

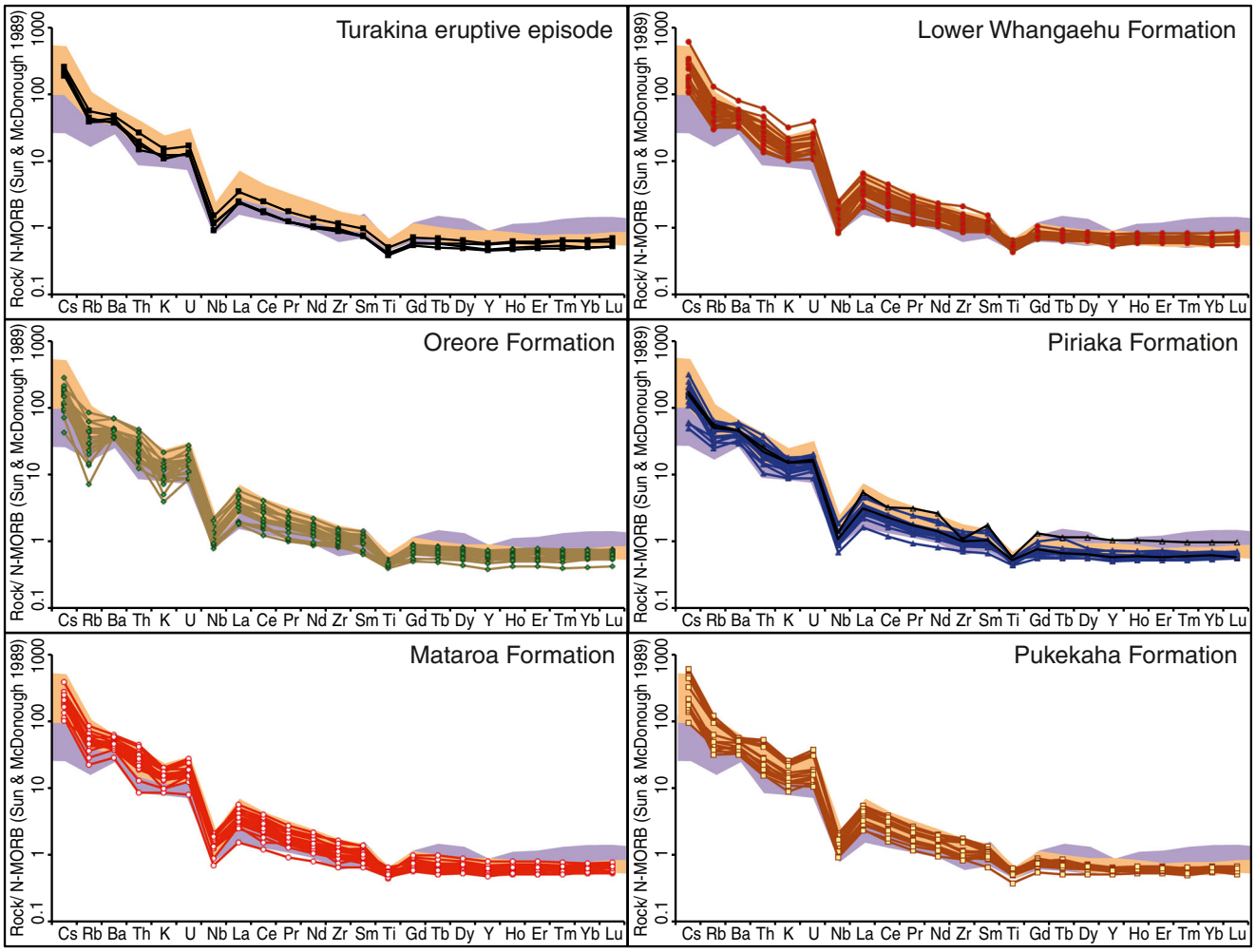

Fig. 8 N-MORB normalized (Sun and McDonough 1989) multi-element plots for lava and pumice clasts from the Ruapehu mass-flow deposits in relation to the lavas of the Te Herenga and Wahianoa cone-building formations exposed on the edifice

that "cryptic amphibole fractionation" did not play a major role in the magma genesis of the stratovolcano.

The Te Herenga eruptive epoch (250–180 ka; Gamble et al. 2003)

The radiometric ages of andesite lava clasts within the Mataroa, Lower Whangaehu and Piriaka Formations indicate that they were formed during the Te Herenga cone-building episode (Tost and Cronin 2015), whereas their geochemical compositions show a strong correlation with the 160–119 ka Wahianoa cone-building formation on Mt. Ruapehu (Gamble et al. 2003) (Fig. 7). A few samples have compositions that overlap with those of the Te Herenga Formation, but the latter is now exposed only on the western and northern sectors of the Ruapehu edifice (Hackett and Houghton 1989) (Fig. 1), and the cone lava flow sample suite may not be representative of the entire eruptive period. The chemical composition of the mass-flow sequences and correlation with the cone lavas suggest that the multi-stage, polybaric magmatic mixing system postulated by Price et al. (2012) for Ruapehu was already established during the Te Herenga cone-building episode, with primitive magmas from the mantle feeding into and stalling within sill- and dyke-like storage systems in the middle and upper crust. These magma batches assimilated meta-igneous and meta-sedimentary crustal material and evolved independently by fractional crystallization. Petrographic textural evidence of magma mixing is absent from the clasts sampled from the Mataroa, Lower Whangaehu and Piriaka Formations.

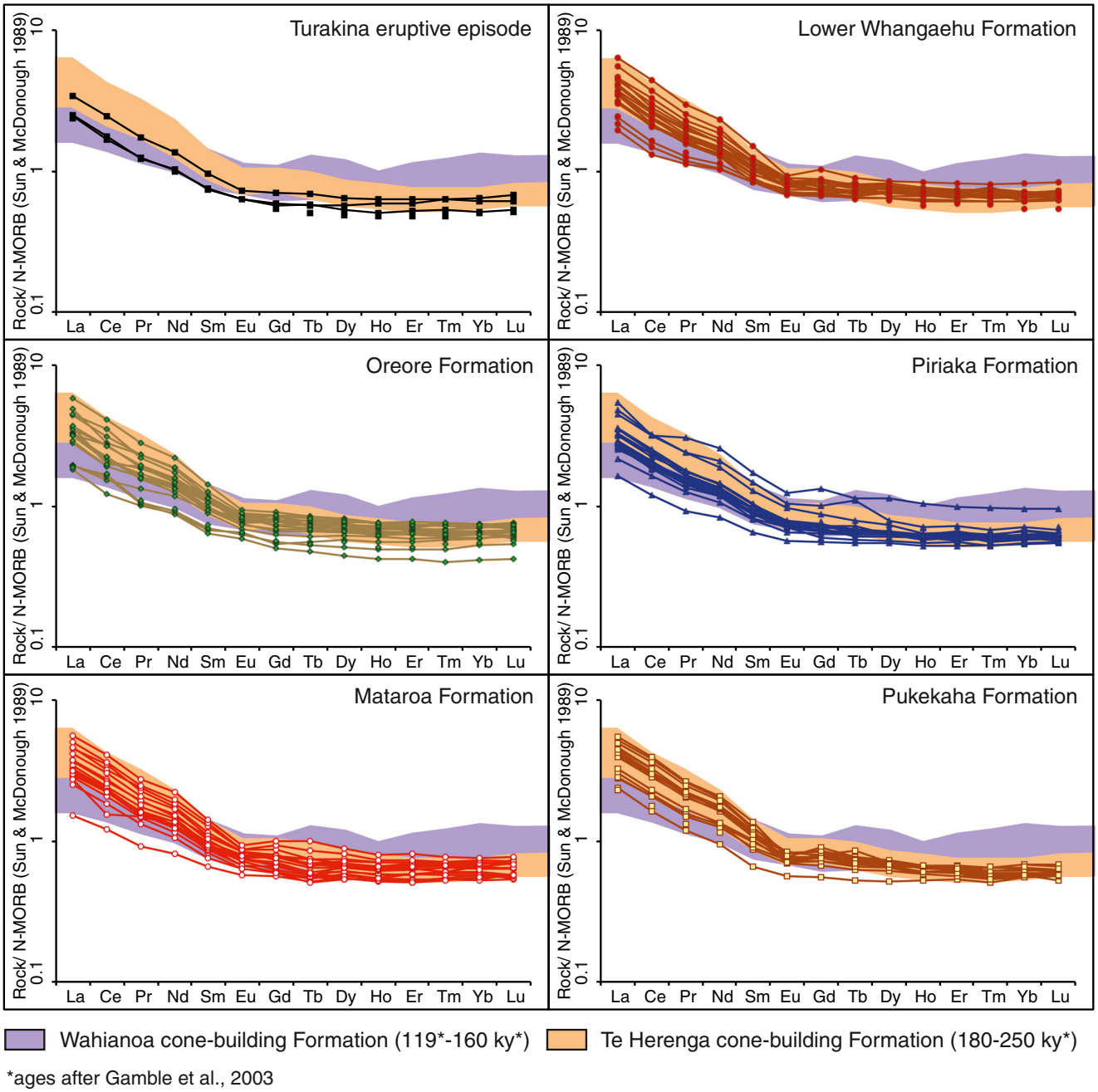

Fig. 9 N-MORB normalized (Sun and McDonough 1989) REE plots for lava and pumice clasts from the Ruapehu mass-flow deposits in relation to the lavas of the Te Herenga and Wahianoa cone-building formations exposed on the edifice

Results from applying the FC-AFC-FCA and mixing modeler of Ersoy and Helvaci (2010), however, indicate that magma mixing was significant (Fig. 11). The partially fused autoliths in basaltic andesites and andesites of the Piriaka Formation may also be evidence for replenishment of the magmatic storage system by hot, mantle-derived melts. Several large-volume flank-collapse-derived debris avalanches (>1 km^3; Tost et al. 2014) occurred at this time, which potentially triggered explosive eruptive activity by unloading Ruapehu's flanks.

The basalts and andesites of the mass-flow suites contain amphibole-free granulitic xenoliths similar to those found in Ruapehu lava flows and corresponding to igneous basement underlying meta-greywacke from the Waipapa and/or Torlesse terranes. The absence of the hornblende-bearing meta-igneous xenoliths in the Ruapehu volcaniclastics following the Turakina eruptive

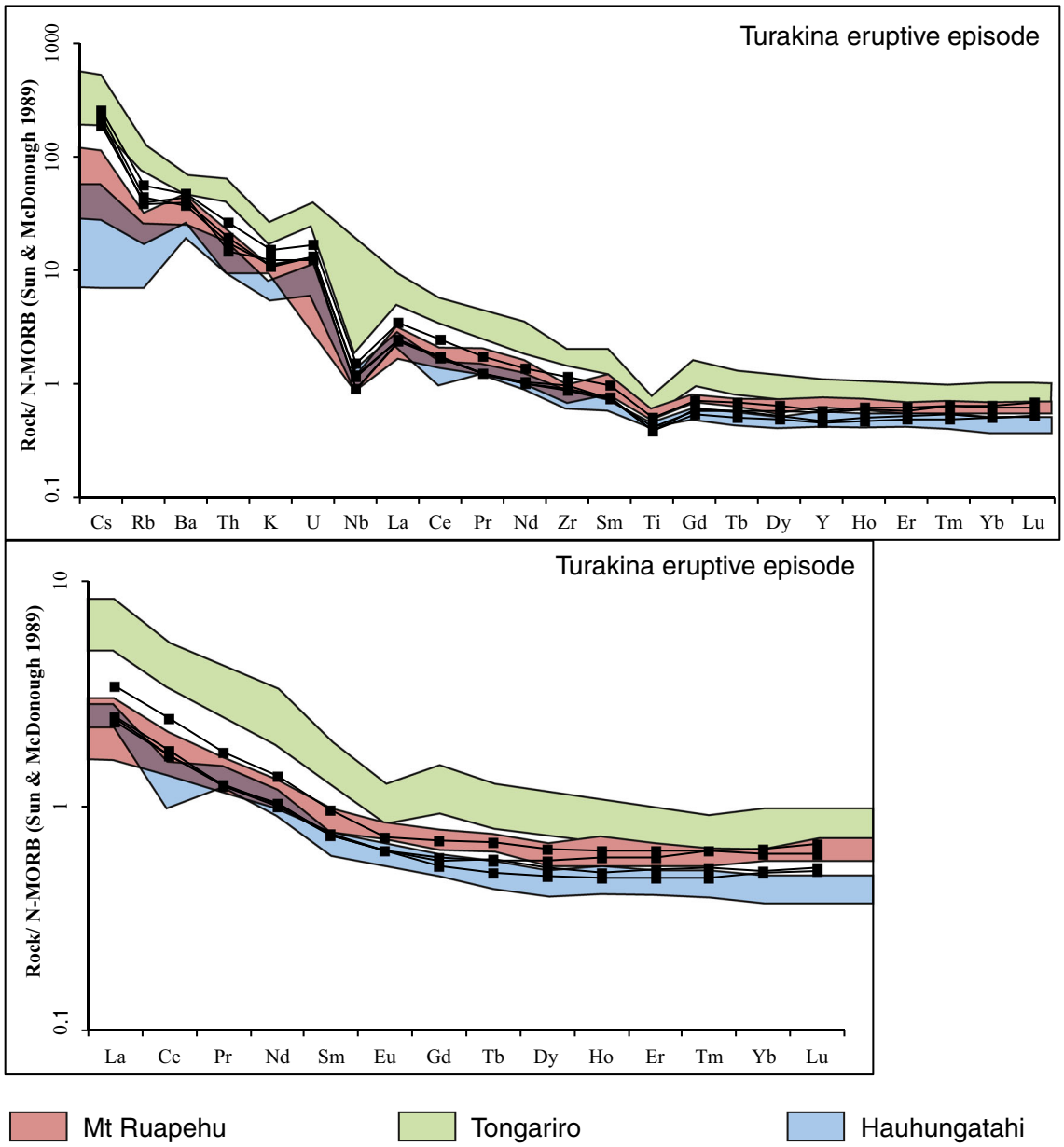

Fig. 10 Trace element composition of pumice clasts from the Turakina eruptive episode compared with those of the lavas exposed on the volcanic edifices of Mt. Ruapehu (Price et al. 2012), Tongariro (Hobden 1997) and Hauhungatahi (Cameron et al. 2010)

interval ~340 ka ago likely indicates a shift of Mt. Ruapehu's main magmatic plumbing system; either to a level where the plutonic material is absent or the physical conditions exceeded the pargasite stabilization field. The prominent pyroxene-mantling of the hornblende xenocrysts might indicate the latter.

The Oreore eruptive epoch (180–160 ka; Tost and Cronin 2015)

Geochemically, the Oreore Formation is the most primitive ($SiO_2 \leq 55$ wt.%) of all the mass-flow sample suites and shows a compositional overlap with the lava flows of the Te Herenga cone-building phase on Mt. Ruapehu (Fig. 7) (Gamble et al. 2003). The geochemistry of the clasts of the Oreore Formation is consistent with the arrival of new primitive, mantle-derived magma into the storage system. The occurrence of two distinct types of groundmass within the mass-flow clast samples indicates that magma mixing may have triggered the onset of this episode. Two samples (KL7 and OH4; supplementary material) have the same petrological characteristics as the samples from the Turakina conglomerate and are likely to represent an older part of the proto-Ruapehu cone that is either now buried or has collapsed away.

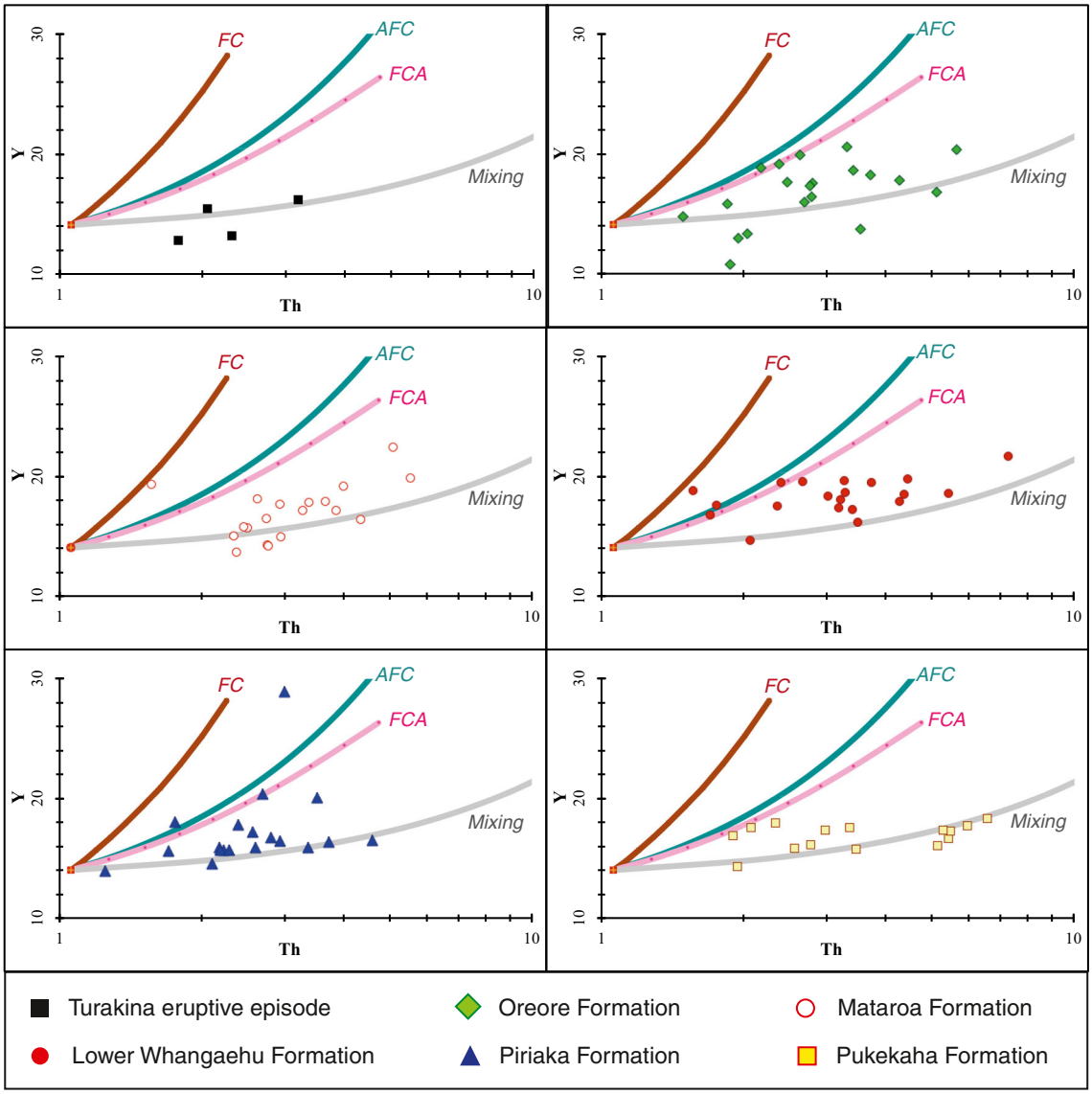

Fig. 11 Model of the dominant magma-modification processes affecting the Mt. Ruapehu melt. Model trajectories were obtained using FC-AFC-FCA (fractional crystallization—assimilation fractional crystallization—fractional crystallization assimilation) and mixing modeler after Ersoy and Helvaci (2010). The relative ratio of assimilated material to crystallized material (r) and the "increments" value indicate that Ruapehu melts were derived from primitive mantle-derived melts subjected to 30 % crystal fractionation and 6 % crustal assimilation (Graham and Hackett 1987). Initial input parameters are listed in the supplementary material

The Waimarino eruptive epoch (100–55 ka; Tost and Cronin 2015)

Dated andesite clasts within the Pukekaha Formation indicate eruption ages ranging between 65.0 ± 10.8 ka and 50.4 ± 10.5 ka (Tost and Cronin 2015). Their chemical composition overlaps closely with the older Wahianoa cone-building lavas on Mt. Ruapehu (160–119 ka; Gamble et al. 2003). The main petrologic difference is that the andesites from the Pukekaha mass-flow deposits have two different groundmass types, showing mingling of magmas. These mingling features, along with the fact that the stratigraphically oldest deposits of the Pukekaha Formation have the highest concentrations of Rb, K, Ba and Zr for any samples with similar silica content, are indications that this period was characterised by vigorous magma recharge and it is, therefore, likely to represent a new cone-building phase.

Conclusions

Reconstructing the complete magmatic history of an active arc stratovolcano or composite cone is challenging, because older

deposits are generally buried by younger volcaniclastic material and lavas on the edifice, or much of the proto-edifice has collapsed and been eroded. Systematic sampling of mass-flow deposits provides the opportunity to expand and extend the magmatic history and thereby gain new insights into the full activity of a volcano and the earliest stages of development of the magmatic system. This approach at Ruapehu volcano has been used to extend the magmatic history by over 90 ka to an onset age of >340 ka, as well as to demonstrate an older initiation time for the Ruapehu magmatic system, i.e. before ~490 ka. The geochemistry of these samples also indicates that, at the earliest stages, the Ruapehu magmatic system became established as a plexus of small-scale storage systems in the mid- to upper crust. Within this dispersed system, primitive mantle-derived magmas were stored, mixed, interacted with crust and evolved along separate polybaric pathways. Magma mingling was common in the earlier history of the stratovolcano, and it may have been associated with recharge events that triggered major phases of eruptive activity, specific individual mass flows and episodes of accelerated cone growth.

The possibility of radiometric dating in distal large-scale mass-flow deposits allows robust chronostratigraphic resolution to interpret changes in eruption behaviour, cone growth and magma-system development. The identification of three previously unknown eruptive epochs (the Turakina, Oreore and Waimarino) provides a framework in which cycles of magmatism that occurred prior to and following the Te Herenga event (250–180 ka; Gamble et al. 2003), and subsequent to the Wahianoa (160–119 ka; Gamble et al. 2003) cone-building episode can be identified. This example from Mt. Ruapehu shows that the geochemical examination of distal mass-flow deposits is an effective tool for building a more complete magmatic evolution of stratovolcanoes, and modification of the underlying basement. Understanding the link between cone-building and collapse phases of the volcano, in relation to features of its magmatic system, helps to improve our understanding of stratovolcano stability and growth/collapse cycles.

Acknowledgments Manuela Tost was supported by a Massey University Doctoral Scholarship and a University of Auckland Doctoral Scholarship. This work is supported by the New Zealand Natural Hazards Research Platform contract "Living with Volcanic Risk" to PI Cronin. We thank Mr Jeff Williams and Mr Rex Martin, along with other farmers for access to their land. We further thank Mr Gordon Holm for the thin section preparation, Mr Jon Wilmshurst for XRF analyses, Dr Anja Moebis for assistance during sample preparation and Dr John Procter for assistance during field studies. We also appreciate useful discussions with Dr Robert Stewart and Dr Alan Palmer regarding the Turakina deposits, and very helpful comments from Dr Adam Martin on an earlier version of this manuscript. We are grateful for the thorough and constructive comments from Dr Steffen Kutterolf, Dr Vern Manville, Prof Vadim Kamenetsky and an anonymous reviewer.

References

Adams CJ, Campbell HJ, Griffin WL (2007) Provenance comparisons of Permian to Jurassic tectonostratigraphic terranes in New Zealand: perspectives from detrital zircon age patterns. Geol Mag 144:701–729

Arculus RJ, Powell R (1986) Source component mixing in regions of arc magma generation. J Geophys Res 91:5913–5926

Arguden AT, Rodolfo KS (1990) Sedimentologic and dynamic differences between hot and cold laharic debris flows of Mayon Volcano, Philippines. Geol Soc Am Bull 102:865–876

Cameron E, Gamble J, Price R, Smith I, McIntosh W, Gardner M (2010) The petrology, geochronology and geochemistry of Hauhungatahi volcano, SW Taupo Volcanic Zone. J Volcanol Geotherm Res 190:179–191

Coats RR (1950). Volcanic activity in the Aleutian arc. US Government Printing Office: 35-49

Cole JW (1978) Andesites of the Tongariro Volcanic Centre, North Island, New Zealand. J Volcanol Geotherm Res 3:121–153

Cole JW, Cashman KV, Rankin PC (1983) Rare-earth element geochemistry and the origin of andesites and basalts of the Taupo Volcanic Zone, New Zealand. Chem Geol 38:255–274

Conway CE, Townsend DB, Leonard GS, Wilson CJN, Calvert AT, Gamble JA (2015) Lava-ice interaction on a large composite volcano: a case study from Ruapehu, New Zealand. Bull Volcanol 77:1–18

Cronin SJ, Neall VE (1997) A late Quaternary stratigraphic framework for the northeastern Ruapehu and eastern Tongariro ring plains, New Zealand. N Z J Geol Geophys 40:185–197

Davidson J, Turner S, Handley H, Macpherson C, Dosseto A (2007) Amphibole "sponge" in arc crust? Geology 35:787–790

Donoghue SL, Neall VE, Palmer AS (1995) Stratigraphy and chronology of late Quaternary andesitic tephra deposits, Tongariro Volcanic Centre, New Zealand. J R Soc N Z 25:115–206

Eggins SM, Rudnick RL, McDonough WF (1998) The composition of peridotites and their minerals: a laser-ablation ICP–MS study. Earth Planet Sci Lett 154:53–71

Ersoy Y, Helvaci C (2010) FC–AFC–FCA and mixing modeler: a Microsoft® Excel© spreadsheet program for modeling geochemical differentiation of magma by crystal fractionation, crustal assimilation and mixing. Comput Geosci 36:383–390

Francis PW, Gardeweg M, Ramirez CF, Rothery DA (1985) Catastrophic debris avalanche deposit of Socompa volcano, northern Chile. Geology 13(9):600–603

Gamble JA, Wood CP, Price RC, Smith IEM, Stewart RB, Waight T (1999) A fifty year perspective of magmatic evolution on Ruapehu Volcano, New Zealand: verification of open system behaviour in an arc volcano. Earth Planet Sci Lett 170:301–314

Gamble JA, Price RC, Smith IEM, McIntosh WC, Dunbar NW (2003) ^{40}Ar-^{39}Ar geochronology of magmatic activity, magma flux and hazards at Ruapehu Volcano, Taupo Volcanic Zone, New Zealand. J Volcanol Geotherm Res 120:271–287

Gerst A, Savage MK (2004) Seismic anisotropy beneath Ruapehu volcano: a possible eruption forecasting tool. Science 306:1543–1547

Graham IJ, Hackett WR (1987) Petrology of calc-alkaline lavas from Ruapehu Volcano and related vents, Taupo Volcanic Zone, New Zealand. J Petrol 28:531–567

Graham IJ, Blattner P, McCulloch MT (1990) Meta-igneous granulite xenoliths from Mt. Ruapehu, New Zealand: fragments of altered oceanic crust? Contrib Mineral Petrol 105:650–661

Graham IJ, Cole JW, Briggs RM, Gamble JA, Smith IEM (1995) Petrology and petrogenesis of volcanic rocks from the Taupo Volcanic Zone: a review. J Volcanol Geotherm Res 68:59–87

Green DH, Hibberson W (1969) Experimental duplication of conditions of precipitation of high pressure phenocrysts in basaltic magma. Phys Earth Planet Inter 3:247–254

Hackett WR, Houghton BF (1989) A facies model for a Quaternary andesitic composite volcano: Ruapehu, New Zealand. Bull Volcanol 51:51–68

Hawkesworth CJ, Gallagher K, Hergt JM, McDermott F (1993) Mantle and slab contribution in arc magmas. Annu Rev Earth Planet Sci 21: 175–204

Hobden BJ (1997). Modelling magmatic trends in time and space: eruptive and magmatic history of Tongariro volcanic complex. Unpublished PhD thesis, University of Canterbury, New Zealand.

Hobden BJ, Houghton BF, Lanphere MA, Nairn IA (1996) Growth of the Tongariro volcanic complex: new evidence from K-Ar age determinations. N Z J Geol Geophys 39:151–154

Houghton BF, Latter JH, Hackett WR (1987) Volcanic hazard assessment for Ruapehu composite volcano, Taupo Volcanic Zone, New Zealand. Bull Volcanol 49:737–751

Houghton BF, Wilson CJN, McWilliams MO, Lanphere MA, Weaver SD, Briggs RM, Pringle MS (1995) Chronology and dynamics of a large silicic magmatic system: central Taupo Volcanic Zone, New Zealand. Geology 23:13–16

Janda RJ, Scott KM, Nolan KM, Martinson HA (1981) Lahar movement, effects, and deposits. US Geol Surv Prof Pap 1250:461–478

Keigler R, Thouret JC, Hodgson KA, Neall VE, Lecointre JA, Procter JN, Cronin SJ (2011) The Whangaehu Formation: debris-avalanche and lahar deposits from ancestral Ruapehu volcano, New Zealand. Geomorphology 133:57–79

Keleman PB, Hanghoj K, Greene AR (2005) One view of the geochemistry of subduction-related magmatic arcs, with an emphasis on primitive andesite and lower crust. In: Rudnick RL (ed) The crust, vol 3, Treatise on Geochemistry. Elsevier Pergamon, Oxford, pp 593–659

Koppers AA (2002) ArArCALC—software for 40Ar/39Ar age calculations. Comput Geosci 28:605–619

Leake BE, Woolley AR, Arps GES, Birch WD, Gilbert MG, Grice JD, Hawthorne FG, Kato A, Kisch HJ, Krivovichev VG, Linthout K, Laird J, Mandarino JA, Maresch WV, Nickel EH, Rock NMS, Schumacher JG, Smith DC, Stephenson NCN, Ungaretti L, Whittaker EJW, Guo YZ (1997) Nomenclature of amphiboles, report of the Subcommitee on amphiboles of the International Mineralogical Association Commission on new minerals and mineral names. Am Mineral 82:1019–1037

LeBas MJ, Lemaitre RW, Streckeisen A, Zanettin B (1986) A chemical classification of volcanic rocks based on the total alkali-silica diagram. J Petrol 27:745–750

Lecointre J, Hodgson KA, Neall VE, Cronin SJ (2004) Lahar-triggering mechanisms and hazard at Ruapehu volcano, New Zealand. Nat Hazards 31:85–109

LeMaitre RW (1989) A classification of igneous rocks and glossary of terms. Blackwell, Oxford, **193 pp**

Lindsley DH (1983) Pyroxene thermometry. Am Mineral 68:477–493

Martin AP, Cooper AF, Price RC (2013) Petrogenesis of Cenozoic, alkalic volcanic lineages at Mount Morning, West Antarctica and their entrained lithospheric mantle xenoliths: lithospheric versus asthenospheric mantle sources. Geochim Cosmochim Acta 122:127–152

McCulloch MT, Gamble JA (1991) Geochemical and geodynamical constraints on subduction zone magmatism. Earth Planet Sci Lett 102: 358–374

Miller V, Savage M (2001) Changes in seismic anisotropy after volcanic eruptions: evidence from Mt. Ruapehu. Science 293:2231–2233

Moore G, Carmichael IS (1998) The hydrous phase equilibria (to 3 kbar) of an andesite and basaltic andesite from western Mexico: constraints on water content and conditions of phenocryst growth. Contrib Mineral Petrol 130:304–19

Mothes PA, Hall ML, Janda RJ (1998) The enormous Chillos Valley Lahar: an ash-flow-generated debris flow from Cotopaxi Volcano, Ecuador. Bull Volcanol 59:233–244

Nockolds SR, Allen R (1954) The geochemistry of some igneous rock series: Part II. Geochim Cosmochim Acta 5:245–285

Norrish K, Hutton JT (1969) An accurate X-ray spectrographic method for the analysis of a wide range of geological samples. Geochim Cosmochim Acta 33:431–453

Palmer BA, Neall VE (1989) The Murimotu Formation—9500 year old deposits of a debris avalanche and associated lahars, Mt. Ruapehu, North Island, New Zealand. N Z J Geol Geophys 32:477–486

Price RC, Waight TE, Chapman JR, Beyer EE, Smith IEM, Stewart RB (1997) The geochemical evolution of arc magmas in a continental setting: evidence from detailed chemo-stratigraphy at Ruapehu, New Zealand. State of the arc'97, Island arc magma genesis workshop, Adelaide, Australia, 1997. Abstr Geol Soc Aust 45:115–117

Price RC, Stewart RB, Woodhead JD, Smith IEM (1999) Petrogenesis of high-K arc magmas: evidence from Egmont volcano, North Island, New Zealand. J Petrol 40:167–197

Price RC, Gamble JA, Smith IEM, Stewart RB, Eggins S, Wright IC (2005) An integrated model for the temporal evolution of andesites and rhyolites and crustal development in New Zealand's North Island. J Volcanol Geotherm Res 140:1–24

Price RC, George R, Gamble JA, Turner S, Smith IEM, Cook C, Hobden B, Dosseto A (2007) U–Th–Ra fractionation during crustal-level andesite formation at Ruapehu volcano, New Zealand. Chem Geol 244:437–451

Price RC, Gamble JA, Smith IEM, Maas R, Waight T, Stewart RB, Woodhead J (2012) The anatomy of an andesite volcano: a time–stratigraphic study of andesite petrogenesis and crustal evolution at Ruapehu Volcano, New Zealand. J Petrol 53:2139–2189

Renne PR, Swisher CC, Deino AL, Karner DB, Owens TL, DePaolo DJ (1998) Intercalibration of standards, absolute ages and uncertainties in $^{40}Ar/^{39}Ar$ dating. Chem Geol 145:117–52

Roser B, Kimura J-I, Sifeta K (2003) Tantalum and niobium contamination from tungsten carbide ring mills: much ado about nothing. Geosci Rep Shimane Univ 22:107–110

Rudnick RL, Gao S (2005) Composition of the continental crust. In: Rudnick RL (ed) The crust, vol 3, Treatise in Geochemistry. Elsevier-Pergamon, Oxford, pp 1–64

Salmon ML, Stern TA, Savage MK (2011) A major step in the continental Moho and its geodynamic consequences: the Taranaki–Ruapehu line, New Zealand. Geophys J Int 186:32–44

Stern T, Stratford W, Seward A, Henderson M, Savage M, Smith E, Benson A, Greve S, Salmon M (2010) Crust–mantle structure of the central North Island, New Zealand, based on seismological observations. J Volcanol Geotherm Res 190:58–74

Stipp JJ (1968). The geochronology and petrogenesis of the Cenozoic volcanics of the North Island, New Zealand. Unpublished PhD thesis, Australian National University Canberra, ACT, Australia.

Stoopes GR, Sheridan MF (1992) Giant debris avalanches from the Colima Volcanic Complex, Mexico: implications for long-runout landslides (>100 km) and hazard assessment. Geology 20:299–302

Sun SS, McDonough W (1989) Chemical and isotopic systematics of oceanic basalts: implications for mantle composition and processes. Geol Soc Lond, Spec Publ 42:313–345

Tatsumi Y, Hamilton DL, Nesbitt RW (1986) Chemical characteristics of fluid phase released from a subducted lithosphere and origin of arc magmas: evidence from high-pressure experiments and natural rocks. J Volcanol Geotherm Res 29:293–309

Tost M, Cronin SJ (2015) Linking distal volcaniclastic sedimentation and stratigraphy with the development of Ruapehu volcano, New Zealand. Bull Volcanol 77:1–17

Tost M, Cronin SJ, Procter JN (2014) Transport and emplacement mechanisms of channelizing long-runout debris avalanches, Ruapehu volcano, New Zealand. Bull Volcanol 76:1–14

Tost M, Cronin SJ, Procter JN, Smith IEM, Neall VE, Price RC (2015) Impacts of catastrophic volcanic collapse on the erosion and morphology of a distal fluvial landscape: Hautapu River, Mt. Ruapehu, New Zealand. Geol Soc Am Bull 127(1-2):266–280

Turner MB, Cronin SJ, Smith IEM, Stewart RB, Neall VE (2008) Eruption episodes and magma recharge events in andesitic systems: Mt Taranaki, New Zealand. J Volcanol Geotherm Res 177:1063–1076

Turner MB, Cronin SJ, Bebbington MS, Smith IEM, Stewart RB (2011) Relating magma composition to eruption variability at andesitic volcanoes: a case study from Mount Taranaki, New Zealand. Geol Soc Am Bull 123:2005–2015

Vallance JW, Scott KM (1997) The Osceola Mudflow from Mount Rainier: sedimentology and hazard implications of a huge clay-rich debris flow. Geol Soc Am Bull 109:143–63

Villamor P, Berryman KR (2006a) Late Quaternary geometry and kinematics of faults at the southern termination of the Taupo Volcanic Zone, New Zealand. N Z J Geol Geophys 49:1–21

Villamor P, Berryman KR (2006b) Evolution of the southern termination of the Taupo Rift, New Zealand. N Z J Geol Geophys 49:23–37

Wager LR, Mitchell RL (1951) The distribution of trace elements during strong fractionation of basic magma—a further study of the Skaergaard intrusion, East Greenland. Geochim Cosmochim Acta 1:129–208

Weaver BL, Tarney J (1984) Major and trace element composition of the continental lithosphere. Phys Chem Earth 15:39–68

Zernack AV, Cronin SJ, Neall VE, Procter JN (2011) A medial to distal volcaniclastic record of an andesite stratovolcano: detailed stratigraphy of the ring-plain succession of south-west Taranaki, New Zealand. Int J Earth Sci 100:1937–1966